

Nonlinear electrodynamics for the vacuum of Dirac materials.

Photon magnetic properties and radiation pressures

A. W. Romero Jorge,^{1,2,3,4,*} A. Pérez Martínez,^{1,†} and E. Rodríguez Querts^{1,‡}

¹*Instituto de Cibernética, Matemática y Física (ICIMAF),
Calle E esq a 15 Vedado 10400 La Habana Cuba*

²*Frankfurt Institute for Advanced Studies,
Ruth Moufang Str. 1, 60438 Frankfurt, Germany*

³*Helmholtz Research Academy Hessen for FAIR (HFHF),
GSI Helmholtz Center for Heavy Ion Physics. Campus Frankfurt, 60438 Frankfurt, Germany*

⁴*Institut für Theoretische Physik, Johann Wolfgang Goethe University,
Max-von-Laue-Str. 1, 60438 Frankfurt, Germany*

(Dated: June 5, 2024)

We investigate the magnetic properties of photons propagating through Dirac materials in a magnetic field, considering both vacuum and medium contributions. Photon propagation properties are obtained through a second-order expansion of non-linear Euler-Heisenberg electrodynamics at finite density and temperature considering Dirac material parameters (Dirac fine structure constant, band gap and Fermi velocity). Total magnetization (including electrons and photon contributions) and photon-effective magnetic moment are computed. Observables such as photon energy density, radiation pressure, and Poynting vector are obtained by an average of components of the energy-momentum tensor. All quantities are expressed in terms of Lagrangian derivatives. Those related to the vacuum are valid for any value of the external magnetic field, and both the weak and strong field limits are recovered. We discuss some ideas of experiments that may contribute to testing in Dirac materials the phenomenology of the strong magnetic field in the quantum electrodynamic vacuum and how non-linear corrections on the magnetization, radiation pressure, and birefringence, are amplified up to 10^3 times QED corrections.

* adrian@icimaf.cu/aromerojorge@physik.uni-frankfurt.de

† aurora@icimaf.cu

‡ elizabeth@icimaf.cu

I. INTRODUCTION

Maxwell's theory predicts that plane-polarized light propagates in a vacuum, or empty space, at the speed of light c . Quantum Electrodynamics (QED), however, presents a different picture of the vacuum. According to this theory, the vacuum is not empty but rather a “sea” of virtual electron-positron pairs, with their negative energy states occupied and positive energy states unoccupied. This model explains how, in the presence of an external magnetic field, the speed of light remains c when propagating parallel to the magnetic field but is lower than c when propagating perpendicular to it. In this case, light changes its plane of polarization, resulting in the wave splitting into two polarized modes that move at different speeds (and frequencies). This phenomenon, known as Cotton-Mouton birefringence, is a consequence of the interaction between the magnetic field and the virtual electron-positron pairs [1, 2].

Viewed through the lens of Quantum Field Theories, the vacuum is considered the ground state of these theories. QED, consists of virtual pairs of electron-positrons, while for Quantum Chromodynamics, it involves virtual quarks-antiquarks. The shift from Maxwell's concept of vacuum to QED's dynamic “sea” of virtual particle pairs redefines its conceptual meaning and aims to understand its properties and complexity.

The vacuum of QED in the presence of a strong electromagnetic field behaves as a medium, and virtual pairs interact with magnetic fields. Thus, the properties of light propagating in a QED vacuum can be studied using nonlinear optic tools, based on Maxwell's theory with all the magnitudes described in terms of a medium electric permittivity and magnetic permeability depending on the non-linear of the external electric and magnetic field¹. Besides birefringence², QED predicts other exotic properties such as the Casimir effect, vacuum instability (close to the critical fields, $B_c = \frac{m^2 c^2}{e\hbar} = 4.41 \times 10^{13}$ G and $E_c = \frac{m^2 c^3}{e\hbar} = 1.3 \times 10^{18}$ V/m, where electron-positron pair creation occurs[4-6]), anisotropy pressures, etc. [7]. All these vacuum phenomena predicted 90 years ago are still awaiting experimental confirmation. Testing the vacuum properties of QED requires large magnetic and/or electric fields. So far, technological barriers limit the generation of such high fields in the laboratory. The magnetic fields achieved in laboratories do not exceed a few teslas (around 5 T= 5×10^4 G) [7, 8]. For instance, vacuum birefringence is a tiny ef-

¹ Vacuum electric permittivity and magnetic permeability are related with the speed of light [3]

² In the presence of a strong electric field, birefringence also appears and is called Kerr birefringence

fect, even though it manifests for any magnetic field strength. At weak field limit, birefringence depends on a quadratic ratio between the magnetic field and the parameter ξ , $\Delta n_{QED} \sim (B/\xi)^2$, where Δn_{QED} defined the difference between the refractive indices of the transverse modes modes³. The Polarization of Vacuum with Laser (PVLAS) experiment [9] was designed to confirm the QED prediction of vacuum birefringence. The strength of the magnetic field of the experiment was 2.5×10^4 G, so $\Delta n_{QED} = 2.5 \times 10^{-23}$, turning into a challenge, its measurement. The experiment was improved, and it obtained a bound close to the prediction $\Delta n_{PVLAS} \sim (12 \pm 17) \times 10^{-23}$ for the same magnetic field [9].

But in the Universe, we can find entities like Neutron stars, whose magnetic fields are close to the critical field, and even more in the case of magnetars [10–12]. Short-time huge magnetic fields may also be found in heavy-ion colliders, which can reach the order of 10^{18} G [13]. In both scenarios, neutron stars and heavy-ion colliders have reported indirect vacuum magnetic birefringence [11, 12]. The work [11] claims the first evidence of vacuum birefringence by measuring the degree and angle of polarization of the photons coming from the pulsar RX J1856.5-4 and comparing them with the theoretical results, but the uncertainties in their measurements are significant enough to trust in this measurement fully.

These observations have boosted the search for the phenomenon directly based on other experimental setups. One plausible alternative is the design of experiments with scattering of the pulsating laser [14]. It is predictable that with the developed technology of lasers, soon, the power of lasers will reach an intensity around $I \sim 10^{28}$ Wm⁻² [15, 16] that corresponds to an electric (magnetic) field close to the critical field, which may allow detection easier the effect of the birefringence of vacuum and to test the pair's creation from the vacuum.

Besides, another exciting and new alternative to probe vacuum properties would be experiments designed with Dirac materials due to their critical fields $E_c = \frac{\Delta^2}{ev_F} \sim 10^3$ V/cm and $B_c = \frac{\Delta^2}{ev_F^2} \sim 10^4$ G = 1 T are accessible in laboratories⁴. A very hopeful work [17] has studied the contribution to the magnetization of the vacuum for three different 3D Dirac materials and the possibility of testing in experiments.

Dirac materials, including Weyl metals, topological materials, and graphene, are characterized by electrons that behave as relativistic fermions with a linear dispersion relation. This

³ $\xi = \frac{8\alpha^2 \hbar^3}{45m^4 c^5} \sim \frac{8\alpha}{45B_c^2}$, with α the fine structure constant.

⁴ where Δ and v_F are the band gap or energy gap and the Fermi velocity of the material respectively.

unique property gives these materials distinctive optical, magnetic, and transport properties. The pioneer theoretical work of Dirac materials is [18], but the boom of these materials only appeared with the fantastic finding of graphene by Novoselov [19]. This experiment led to a boom of experimental and theoretical work to look for other materials or properties, and consequently, to technological applications.

The discovery of Dirac materials has been gratifying news for the Quantum Field Theory because it has opened the window to test in top-table experiments, theories, and phenomena requiring a large scale of energies and expensive experiments in particle accelerators [20]. Consequently, the tools of Quantum Field theory have been extended to condensed matter physics. In line with this direction, the investigation of photon propagation parallel to an external magnetic field in electron-positron plasma [21–23] was expanded to include graphene-like systems. This extension encompassed the study of the Faraday and Quantum Hall effects [24–26]. Leveraging previous calculations [21–23] from one-loop QED perturbative studies of 3D electron-positron plasma in a magnetized medium, a “dimensional reduction” to 2D was performed while also considering the specific properties of graphene-like systems. In this paper, we proceed similarly extrapolating to Dirac materials physics, the results of the study of photon propagation transverse to the external magnetic field. We have used the extended to finite temperature and density of the effective Euler-Heisenberg (EH) non-linear electrodynamics to study the properties of electron-hole plasma. In particular, we use an approximated version of the extended EH Lagrangian, which corresponds to an expansion up to second order on the photon field [27] in the limit of $\omega \ll 2mc^2$, where m is the electron mass. From this Lagrangian, we investigate the magnetic and dielectric properties of a photon traveling in the Dirac vacuum and the observables, energy densities and pressures, and Poynting vector resulting from the energy-momentum tensor. We also study the magnetic properties of Dirac materials in the medium and compare them with those of photons, finding that they are the primary contributors to overall magnetization.

Our work introduces several novel aspects that deserve highlighting. Firstly, we extend the effective Euler-Heisenberg action to finite density and temperature to discuss the magnetic properties of 3D Dirac materials. Additionally, we examine the magnetization of photons propagating transverse to an external magnetic field. To achieve this, we expand the Euler-Heisenberg Lagrangian up to the second order on the photon field, considering non-linear contributions from both vacuum and medium. This approach allows us to derive

the magnetization of the Dirac materials described by electrons (Dirac vacuum and medium) as a zero-order term of the expansion and the magnetization of photons interacting with the magnetic field via the vacuum or medium. Secondly, we consider the photons propagating in a Dirac vacuum while accounting for arbitrary magnetic field values, which allows for the recovery of both weak and strong magnetic field limits. Thirdly, we calculate the energy-momentum tensor and observables for photons propagating in the vacuum in terms of derivatives of the effective Lagrangian. This formulation makes it possible to extend our approach straightforwardly to other non-electrodynamics. Furthermore, the extension of this calculation to finite temperature and density is also straightforward.

Furthermore, our study is also essential for the interest that awakens the magnetic properties of Dirac materials (including the vacuum properties) and for eventually testing the properties of the strong field QED regime. As we have already commented, critical fields for the Dirac materials are experimentally reachable. Hence, these materials could imitate the birefringence, anisotropic pressures, and other exotic properties of the vacuum of QED at the regime of the strong magnetic field.

The paper is organized as follows: in Sec. II, a brief overview of Dirac materials characteristics is illustrated. In Sec. III, we extrapolate the extended effective Lagrangian of QED in the presence of electromagnetic fields to 3D Dirac materials. Sec. IV, is devoted to studying the electron and photon magnetic properties in the presence of an external magnetic field. In Sec. V, we calculate the photon magnetic moment. The solution of the Maxwell equation and dispersion equation of photon propagating in the 3D Dirac vacuum is presented in Sec. VI. In Sec. VII, the energy-momentum tensor is presented, and observables like energy density pressures and Poynting vector are obtained. Finally, we conclude the work, and some calculations are presented in the appendixes. We used natural units in the paper, except for some cases for clarity.

II. A BRIEF OVERVIEW OF DIRAC MATERIALS CHARACTERISTICS

The crystalline structure of Dirac materials is characterized by a “Dirac points” or well, with a small band gap around them, the electrons behave like relativistic particles with free electrons as Dirac fermions exhibiting an extremely high Fermi speed, about 10^6 m/s and electrons could be described by a linear relationship according to $\epsilon \approx v_F p$ between the

energy and momentum of its electrons in the conduction and valence band for low energies [17, 28]. Dirac materials with zero mass (gap) are known as Weyl fermions, and the very well-known is graphene [29]. This one, a highly conductive material with no energy gap in its Dirac points ($\Delta = 0$), it is distinguished from conventional semiconductors by its absence of this gap ($\Delta \neq 0$). These energy gaps can be controlled by manipulating the width of the graphene ribbon and introducing defects or doping, among other factors. By employing these techniques, small energy gaps are observed, ranging approximately from 100 meV to 250 meV [30–34]. Our study considers a non-zero gap graphene energy with an energy gap of 100 meV [35].

Formally, graphene is not a 2D Dirac semimetal actually, with the top of the valence and bottom of the conduction band of a band The insulator just touches before gapping up again after band inversion, resulting in a graphene-like semimetallic state. Besides graphene and topological insulators with 2D Dirac surface states, there is a 3D semimetal with a Dirac point in the bulk 3D Brillouin zone linear dispersion in all three k directions. The theoretical prediction and the experimental proof in Bi-based materials did not take long [36–39]. These materials are also called (3D) Dirac semimetals.

Our study will focus on these materials by considering a simple model. We know that the crystal structure of these materials is sufficiently complicated with various nodes, but as a first approximation, we consider the following points:

1. All nodes are equal and we assume a constant energy gap independent of all the parameters of the material.
2. We neglect the contribution to magnetization due to material impurities.
3. We are assuming that the properties of the materials are stable for values of the magnetic/electric field above the critical field of each material.

With this model, we will proceed to study the propagation of photons, extrapolating the results of QED, to 3D Dirac materials. It means shifting the values of the critical fields in Dirac materials are defined as [17, 28]

$$E_c(\Delta, v_F) = v_F B_c(\Delta, v_F) = \frac{\Delta^2}{ev_F}, \quad (1)$$

where the speed of light has been replaced by the Fermi velocity of the material ($c \rightarrow v_F \approx 10^6$ m/s), the fine structure constant has been changed to an effective or Dirac fine structure

constant ($\alpha \rightarrow \alpha_D$) defined as $\alpha_D = e^2/v_F \sim 1 - 4$. Here the band gap or energy gap of the material is defined as $\Delta = m^*mv_F^2$, where $m^* \sim 0.01 - 0.5$ is the effective mass of electrons and holes [17, 28].

Table I presents a comparison of QED and four materials that we use in our study: graphene, tantalum arsenide (Ta_3As_4), bismuth antimony ($Bi_{1-x}Sb_x$), and lead tin tellurium ($Pb_{1-x}Sn_xTe$). Also, we have listed the values of $3\pi/\alpha_D$ for each material, which are related to the maximum allowed values of the magnetic field to get accurate corrections to phase velocity in the strong field limit $v_p^2 \approx 1 - \frac{\alpha_D}{3\pi}b > 0$, where $b = B_e/B_c$, B_e is the external constant magnetic field and $b_{max} = 3\pi/\alpha_D$. This bound ensures the validity of one-loop approximation and the effective non-linear electrodynamics [27, 40], above this strength, we have to include two-loop corrections.

	Δ (meV)	α_D/α	B_c (T)	E_c (V/cm)	b_{max}
QED	10^9	1	4.4×10^9	1.3×10^{16}	1291
$Pb_{1-x}Sn_xTe$	31.5	580	5.6	2.9×10^4	2.22
$Bi_{1-x}Sb_x$	7.75	188	0.036	5.7×10^2	6.86
Ta_3As_4	21	357	0.95	7.9×10^3	3.61
Graphene	100	301	15.4	1.5×10^5	4.28

Table I. Comparison of QED and four Dirac materials for different parameters like band gap (Δ), Dirac structure constant (α_D) over α , critical magnetic field (B_c), critical electric field (E_c), and bound of the dimensionless external magnetic field $b = B_e/B_c$ imposed to ensure the validity of non-linear electrodynamics. Some values of QED are listed as a reference and the Dirac materials: $Pb_{1-x}Sn_xTe$ [17, 28, 41, 42], $Bi_{1-x}Sb_x$ [17, 28, 42, 43], Ta_3As_4 [17, 28, 44], and graphene [19, 25, 35].

Each material will be defined only by its Fermi speed and energy gap so that several materials can have the same characteristics. We are referring, for example, to the graphene-type material that has its Fermi speed and energy gap given, but it can be another material with the same characteristics.

III. NLED FOR DIRAC MATERIALS, LAGRANGIAN

In this section, we extrapolate the extended effective Lagrangian of QED in the presence of electromagnetic fields to 3D Dirac materials. The extending effective Lagrangian

corresponds to considering finite temperature and density and the possibility of evaluating thermodynamical potential in the presence of external and constant magnetic fields. Besides, we can study the propagation of photons in 3D materials by doing an expansion of the effective Lagrangian up to the second order of the photon fields. This treatment allows us to calculate the magnetization of the electrons (zero-order of the expansion) and photons (terms of the first and second order of the expansion) and consider both the vacuum and medium contribution.

We start from the Lagrangian of QED where fermions are coupled with an electromagnetic vector field A_μ ⁵,

$$\mathcal{L}(\bar{\psi}, \psi, A_\mu) = \bar{\psi}(\not{\partial} - e\not{A}_\mu - m)\psi + \frac{1}{4}F_{\mu\nu}F^{\mu\nu}, \quad (2)$$

where $\bar{\psi}$, ψ are the fermion spinors, $\not{\partial} = \gamma^\nu \partial_\nu$, $\not{A}_\mu = \gamma^\mu A_\mu$, γ_μ are the Dirac matrices, A_μ is the cuatri-potential vector of the electromagnetic field and $F_{\mu\nu}$ is the electromagnetic tensor. We start from the grand partition function defined as $Z = Tr\{e^{k_B T(H - \mu N)}\}$, where k_B is the Boltzmann constant, T is the temperature, H is the Hamiltonian, μ is the chemical potential, and N is the number of particle density. The partition function in the path integral language corresponds to

$$Z = \int \mathcal{D}\bar{\psi} \mathcal{D}\psi e^{ik_B T \int_0^1 d\tau \int d^3x \mathcal{L}(A_\mu, \psi)}, \quad (3)$$

where we use Euclidean space-time with $\tau = it$ a variable in the interval 0 to $k_B T$.

In one-loop approximation, the effective Lagrangian at finite temperature and density⁶ in the presence of an electromagnetic field reads as,

$$\mathcal{L}_{eff} = k_B T Tr\{\ln Z\} = ik_B T \ln \det G^{-1}(x, x'), \quad (4)$$

where $G^{-1}(x, x')$ is the inverse electron Green function in the presence of electromagnetic fields and determinant and logarithm are functional operations. Doing the functional operations over the propagator in integral representation, following the steps described in [40, 45, 46] from Eq. (4) one arrives to the general effective Lagrangian [40, 45, 46]

$$\begin{aligned} \mathcal{L}_{eff}(\tilde{a}, \tilde{b}, \mu, T) = & -\mathcal{F} - \frac{1}{8\pi^2} \int_0^{i\infty} \frac{ds}{s^3} e^{-i(m^2 - i\epsilon)s} \\ & \times \left[(es)^2 \tilde{a}\tilde{b} \coth(e\tilde{a}s) \cot(e\tilde{b}s) \right] \left(1 + 2 \sum_{k=1}^{\infty} e^{-\frac{iek^2\beta^2}{4}h(s, \tilde{a}, \tilde{b})} \cosh(\mu\beta k) \right), \end{aligned} \quad (5)$$

⁵ We used Minkowski flat space with the convention $g_{\mu\nu} = \eta_{\mu\nu} = \{+1, -1, -1, -1\}$

⁶ The thermodynamical potential of the electron-hole plasma is $\Omega = \mathcal{L}_{eff}$

where $\beta = 1/k_B T$, $\tilde{a} = [(\mathcal{F}^2 + \mathcal{G}^2)^{1/2} + \mathcal{F}]^{1/2}$, $\tilde{b} = [(\mathcal{F}^2 + \mathcal{G}^2)^{1/2} - \mathcal{F}]^{1/2}$, \mathcal{F} and \mathcal{G} are the secular invariants derived from the gauge and Lorentz invariants of the generic electromagnetic fields (\mathbf{E} , \mathbf{B})

$$\mathcal{F} = \frac{1}{4} F^{\mu\nu} F_{\mu\nu} = \frac{1}{2} (-\epsilon_0 E_e^2 + \frac{B_e^2}{\mu_0}), \quad (6)$$

$$\mathcal{G} = \frac{1}{4} F^{\mu\nu} \tilde{F}_{\mu\nu} = \sqrt{\frac{\epsilon_0}{\mu_0}} (-\mathbf{E}_e \cdot \mathbf{B}_e), \quad (7)$$

where μ_0 and ϵ_0 are electrical permittivity and magnetic permeability respectively⁷. $E_{e,(i)}$ and $B_{e,(i)}$ are the components of electromagnetic tensors defined as $E_{e,(i)} = F_{0i}$, $B_{e,(i)} = -\frac{1}{2} \epsilon_{ijk} F^{jk}$ with $i = 1, 2, 3$, $\tilde{F}^{\mu\nu} = \epsilon^{\mu\nu\alpha\beta} F_{\alpha\beta}/2$ is the dual tensor, and $\epsilon^{\mu\nu\alpha}$ and $\epsilon^{\mu\nu\alpha\beta}$ are the totally antisymmetric Levi-Civita tensors of rank 3 and 4, respectively.

The first term of the effective Lagrangian is the unrenormalized non-linear EH Lagrangian, while the second one corresponds to the temperature and density correction. In a medium, Lorentz symmetry is broken, and the reference frame would be specified by the medium velocity u_μ . Hence, the general effective Lagrangian apart of the electromagnetic field invariants \tilde{a} , \tilde{b} includes $u_\mu = (1, 0, 0, 0)$ by the covariant form of the electric field $E_e^\mu = F^{\mu\nu} u_\nu$, $E_e^\mu = (0, \mathbf{E}_e)$ so that $\varepsilon_u^2 = |\mathbf{E}_e|^2$. The function $h(s)$ that appears in the exponent of the second term is

$$h(s, \tilde{a}, \tilde{b}) = \tilde{a} \frac{\tilde{b}^2 + \varepsilon_u^2}{\tilde{a}^2 + \tilde{b}^2} \cot(e\tilde{a}s) + \tilde{b} \frac{\tilde{a}^2 - \varepsilon_u^2}{\tilde{a}^2 + \tilde{b}^2} \coth(e\tilde{b}s), \quad (8)$$

and it relates the electromagnetic invariants with medium velocity (details of the extended effective Lagrangian could be seen in [40, 45, 46]).

The effective Lagrangian Eq (5) is reduced to constant external magnetic field taking $\tilde{b} \rightarrow 0$ and $\mathcal{G} = 0$ ($E_e = 0$) leaving only the invariant $\mathcal{F} = B_e^2/2$.

In that case, the first term of the Lagrangian depends only on the magnetic field, while the second term additionally depends on temperature and chemical potential, with

$$\mathcal{L}_{eff}(B_e) = -\frac{1}{8\pi^2} \int_\epsilon^\infty \frac{ds}{s^3} \left(2e^{-m^2 s} (eB_e s) \coth(eB_e s) \right), \quad (9)$$

$$= \frac{eB_e}{4\pi^2} \int_{-\infty}^\infty dp_3 \sum_{\sigma, n} |E_{\sigma n}|, \quad (10)$$

⁷ Along the paper, by simplicity, we take $\mu_0 = \epsilon_0 = 1$

where $\mathcal{L}_{eff}(B_e)$ has to be renormalized and with the Maxwell classical terms we get the Euler-Heisenberg effective non-linear Lagrangian [4]. Its expression is

$$\mathcal{L}_{eff}^R(B_e) = -\mathcal{F} - \frac{1}{8\pi^2} \int_{\epsilon}^{\infty} \frac{ds}{s^3} \left(2e^{-m^2s} (eB_e s) \coth(eB_e s) - 1 - \frac{(eB_e s)^2}{3} \right). \quad (11)$$

The $\mathcal{L}_{eff}(B_e, T, \mu)$ remains as [40]

$$\mathcal{L}_{eff}(B_e, \mu, T) = -\frac{1}{8\pi^2} \int_{\epsilon}^{\infty} \frac{ds}{s^3} 2e^{-m^2s} ((eB_e s) \coth(eB_e s)) \left(\sum_{k=1}^{\infty} e^{-\frac{ek^2\beta^2}{4s}} \cosh(\mu\beta k) \right) \quad (12)$$

$$= \frac{eB_e}{4\pi^2} \int_{-\infty}^{\infty} dp_3 \sum_{\sigma, n} \frac{1}{\beta} \ln(1 + e^{-\beta|E_{\sigma n} - \mu|})(1 + e^{-\beta|E_{\sigma n} + \mu|}), \quad (13)$$

where $E_{\sigma n} = \sqrt{p_3^2 + m^2 + eB_e(2n + 1 + \sigma)}$, σ is the spin and the number k corresponds to the sum over the Matsubara frequencies.

We can analyze their contributions separately as

$$\mathcal{L}_{eff}(B_e, T, \mu) = \mathcal{L}_{eff}^R(B_e) + \mathcal{L}_{eff}(B_e, T, \mu). \quad (14)$$

We want to point out that Eq. (10) and (13) show the equivalence in one loop of the effective Lagrangian [45] obtained by proper time Schwinger method Eq. (9) and (12) respectively and the obtained using the functional approach in imaginary time formalism for electron propagator interacting with the magnetic field at finite temperature and density [47]. (The appendix (A) provides details on how to transition from one to the other). Although both representations are equivalent, depending on the specific calculation, one might be more advantageous than the other. For instance, the integral representation using the proper time method is simpler for regularizing the effective Lagrangian. Conversely, for calculating integrals at the limit of zero temperature and non-zero chemical potential, the partition function of electron-positrons is more suitable and straightforward.

Usually, when one studies electron-positron plasma in an external magnetic field, the vacuum contribution is ignored because it is only relevant close to the critical field. However, for Dirac materials, the critical fields are reachable in laboratories, so studying the relevance and the presence of their contribution is very timely for backing up the QED vacuum properties.

Let's move to Dirac material language. Without loss of generality [17, 28], we change m and α in the effective Lagrangian by Δ and α_D Eq. (5)-(13), i.e. from now on $\mathcal{L}_{eff} \rightarrow \mathcal{L}_D(\alpha_D, \Delta)$.

Experiments on Dirac materials typically involve densities higher than temperatures of around 10^2 meV, while the temperatures are approximately 10 K (< 1 meV) [42, 44]. So, the degenerate limit ($T \ll \mu$) is suitable, holes are neglected and the integral over p_3 in Eq. (13) yields the following expression for the effective Lagrangian [48]

$$\mathcal{L}_D = \frac{e\Delta^2}{4\pi^2 v_F} \sum_{n=0}^{n_\mu} a_n b \int |E'_{\sigma n} - \mu'| \theta(E'_{\sigma n} - \mu') dp'_3, \quad (15)$$

$$= \frac{e\Delta^2}{4\pi^2 v_F} \sum_{n=0}^{n_\mu} a_n b \left(\mu' p'_f - (1 + 2nb) \ln \left(\frac{\mu + p_f}{\Delta_n} \right) \right), \quad (16)$$

where $a_n = 2 - \delta_{0n}$, $b = B_e/B_c$, $dp'_3 = dp_3/\Delta$, $E'_{\sigma n} = \sqrt{p_3^2/\Delta^2 + 1 + (2n + 1 + \sigma)b}$, $\mu' = \mu/\Delta$, $p'_f = 1/v_F \sqrt{\mu'^2 - \Delta_n'^2}$, $\Delta_n'^2 = 1 + 2nb$, $p_f = 1/v_F \sqrt{\mu^2 - \Delta_n^2}$ is the Fermi momentum, $\Delta_n^2 = \Delta^2 + 2eBn v_F$, and n_μ is the maximum number of Landau levels taken from the integer part of $n_\mu = \frac{\mu^2 - \Delta^2}{2eB_e v_F} = \frac{\mu^2 - 1}{2b}$.

A. Photon propagation in the presence of a constant magnetic field

We aim to investigate the properties of photons propagating perpendicular to an external and constant magnetic field along the x_3 -direction in a 3D Dirac material. To undertake this study, we employ non-linear electrodynamics (non-perturbative QED), beginning with the extension of Euler-Heisenberg's effective Lagrangian to finite temperature and density regimes in the infrared limit ($\omega \ll 2m^2$).

Therefore, we start from effective Lagrangian Eq. (5) making the prescription for the vector potential [27]: $A_\mu = A_\mu^{ext} + a_\mu$, where a_μ represents the four-potential of the photon and A_μ^{ext} is the potential associated with the external and constant magnetic field \mathbf{B}_e and the corresponding electromagnetic field tensor is $\mathcal{F}_{\mu\nu} = f_{\mu\nu} + \mathcal{F}_{\mu\nu}^B$ where

$$f_{\mu\nu} = \partial^\mu a^\nu - \partial^\nu a^\mu, \quad \mathcal{F}_{\mu\nu}^B = \partial^\mu A^{ext,\nu} - \partial^\nu A^{ext,\mu}, \quad (17)$$

with $\mathbf{B} = \mathbf{B}_e + \mathbf{B}_w$ and $\mathbf{E} = \mathbf{E}_w$, where B_w and E_w are the wave magnetic and electric field respectively. The invariants become in

$$\mathcal{F} = \frac{1}{4} F^{\mu\nu} F_{\mu\nu} + \frac{1}{4} f^{\mu\nu} f_{\mu\nu} = \frac{1}{2} (-E_w^2 + B_w^2) + \frac{B_e^2}{2}, \quad (18)$$

$$\mathcal{G} = \frac{1}{4} F^{\mu\nu} \tilde{F}^{\mu\nu} + \frac{1}{4} f^{\mu\nu} \tilde{f}^{\mu\nu} + \frac{1}{4} f^{\mu\nu} \tilde{F}^{\mu\nu} + \frac{1}{4} F^{\mu\nu} \tilde{f}^{\mu\nu} = -\mathbf{E}_w \cdot \mathbf{B}_e. \quad (19)$$

As the photon propagates in constant magnetic field, $E \rightarrow 0$, i.e. and $\tilde{b} \rightarrow 0$ and $h(s) = 1/s$. We expand up to the second order of the photon fields the extended effective Euler Heisenberg Lagrangian [27, 40].

The explicit expression of the expansion has the form

$$\mathcal{L}_D(B_e, E_w, B_w, T, \mu) = \mathcal{L}_D^{(e-B_e)}(B_e, T, \mu) |_{E_w=B_w=0} + \mathcal{L}_D^{(ph)}(B_e, E_w, B_w, T, \mu), \quad (20)$$

where $\mathcal{L}_D^{(e-B_e)}(B_e, T, \mu) |_{E_w=B_w=0}$ is the zero order of the expansion, and it corresponds to the effective Euler Heisenberg Lagrangian for electrons in the presence of constant magnetic field written in the previous heading as Eq. (10) and (13), $\mathcal{L}_D^{(e-B_e)}(B_e, T, \mu) |_{E_w=B_w=0} = \mathcal{L}_D^R(B_e) + \mathcal{L}_D(B_e, T, \mu)$, while $\mathcal{L}_D^{(ph)}(B_e, E_w, B_w, T, \mu)$ is a quadratic non-linear effective Lagrangian and it contents interaction of photons with the magnetic field via virtual pairs (vacuum) and through electrons (medium) and, in the considered approximation, looks like

$$\mathcal{L}_D^{(ph)} = \frac{1}{4}(1 - \mathcal{L}_{\mathcal{F}}^{f,D})f^{\mu\nu}f_{\mu\nu} + \frac{\mathcal{L}_{\mathcal{F}\mathcal{F}}^{f,D}}{8}(f^{\mu\nu}F_{\mu\nu}^B)^2 + \frac{\mathcal{L}_{\mathcal{G}\mathcal{G}}^{f,D}}{8}(f^{\mu\nu}\tilde{F}_{\mu\nu}^B)^2, \quad (21)$$

where the coefficients of the expansion are $\mathcal{L}_{\mathcal{F}}^{f,D} = \mathcal{L}_{\mathcal{F}}^D + \mathcal{L}_{\mathcal{F}}^{(\mu,T),D}$, $\mathcal{L}_{\mathcal{F}}^D$ is the renormalized EH effective action Eq. $\mathcal{L}_{\mathcal{F}\mathcal{F}}^{f,D} = \mathcal{L}_{\mathcal{F}\mathcal{F}}^D + \mathcal{L}_{\mathcal{F}\mathcal{F}}^{(\mu,T),D}$, $\mathcal{L}_{\mathcal{G}\mathcal{G}}^{f,D} = \mathcal{L}_{\mathcal{G}\mathcal{G}}^D + \mathcal{L}_{\mathcal{G}\mathcal{G}}^{(\mu,T),D}$.

The presence of finite temperature and density, which characterize the medium, appear as temperature and density-dependent expansion coefficients in addition to those that depend solely on the magnetic field, such as $\mathcal{L}_{\mathcal{F}}^D$, $\mathcal{L}_{\mathcal{F}\mathcal{F}}^D$, and $\mathcal{L}_{\mathcal{G}\mathcal{G}}^D$. These latter are regularized integrals dependent on arbitrary values of the external magnetic field [27, 40, 49–51]. They represent quantum corrections up to second order to the classical Lagrangian photon field $f^{\mu\nu}f_{\mu\nu}$, proportional to α_D . We can rewrite Eq. (21) by separating the vacuum from the medium photon interaction, $\mathcal{L}_D^{(ph)} = \mathcal{L}_D^{(ph-B_e)} + \mathcal{L}_D^{(ph-B_e-e)}$ where

$$\mathcal{L}_D^{(ph-B_e)} = \frac{1}{4}(1 - \mathcal{L}_{\mathcal{F}}^D)f^{\mu\nu}f_{\mu\nu} + \frac{\mathcal{L}_{\mathcal{F}\mathcal{F}}^D}{8}(f^{\mu\nu}F_{\mu\nu}^B)^2 + \frac{\mathcal{L}_{\mathcal{G}\mathcal{G}}^D}{8}(f^{\mu\nu}\tilde{F}_{\mu\nu}^B)^2, \quad (22)$$

$$\mathcal{L}_D^{(ph-B_e-e)} = \frac{1}{4}\mathcal{L}_{\mathcal{F}}^{(\mu,T),D}f^{\mu\nu}f_{\mu\nu} + \frac{\mathcal{L}_{\mathcal{F}\mathcal{F}}^{(\mu,T),D}}{8}(f^{\mu\nu}F_{\mu\nu}^B)^2 + \frac{\mathcal{L}_{\mathcal{G}\mathcal{G}}^{(\mu,T),D}}{8}(f^{\mu\nu}\tilde{F}_{\mu\nu}^B)^2. \quad (23)$$

The integrals concerning Lagrangian derivatives are outlined in the appendix (A 1) and (A 2). For a detailed explanation of the calculations, see [40, 45].

Let us note that all the Lagrangians Eqs. (5), (21) and (23) preserve the parity conservation, because there are no odd powers of the invariant \mathcal{G} in these expressions, since both coefficients $\mathcal{L}_{\mathcal{F}\mathcal{G}} = \mathcal{L}_{\mathcal{G}} = 0$.

IV. MAGNETIC PROPERTIES OF PHOTON PROPAGATION IN DIRAC MATERIALS. MAGNETIZATION

Let us start from Eq. (20) to study the total magnetization resulting from electrons and photons interacting with the magnetic field via vacuum (virtual pairs) and medium (electrons). This is obtained by $\mathcal{M}^{(T)}(B_e) = -\frac{\partial \mathcal{L}_D}{\partial \mathbf{B}_e}$ [25] and it has the form

$$\mathcal{M}^{(T)} = \mathcal{M}^{(e)}(B_e, T, \mu) + \mathcal{M}^{(ph)}(B_e, T, \mu), \quad (24)$$

$$\mathcal{M}^{(e)}(B_e, T, \mu) = \mathcal{M}^{(B_e)}(B_e) + \mathcal{M}^{(e-B_e)}(B_e, T, \mu), \quad (25)$$

$$\mathcal{M}^{(ph)}(B_e, T, \mu) = \mathcal{M}^{(ph-B_e)}(B_e) + \mathcal{M}^{(ph-B_e-e)}(B_e, T, \mu). \quad (26)$$

In the degenerate gas limit (at finite density and zero temperature), the Dirac material magnetization (due to electrons) can be calculated from Eq. (16) and it reads as

$$\mathcal{M}^{(e-B_e)}(B_e, \mu) = \mathcal{M}_0 \sum_{n=0}^{n_\mu} \frac{3a_n}{2} \left(\mu' p'_F - (1 + 4nb) \ln \left(\frac{\mu + p_f}{\Delta_n} \right) \right), \quad (27)$$

where $\mathcal{M}_0 = e\Delta^2 / (6\pi^2 v_F)$ [48]. The corresponding magnetization of the vacuum is obtained from Eq. (9), which arises from the interaction of virtual pairs with the magnetic field. The integral can be solved for weak (WF) and strong field (SF) limits, yielding

$$\mathcal{M}^{(B_e)SF}(B_e) = \mathcal{M}_0 b(\ln(b) + 1), \quad \mathcal{M}^{(B_e)WF}(B_e) = \mathcal{M}_0 b^3. \quad (28)$$

This vacuum magnetization $\mathcal{M}^{(B_e)}(B_e)$ agrees with [17] for $E_e = 0$.

Photon magnetization due to the photon interaction with the vacuum is

$$\mathcal{M}^{(ph-B_e)}(B_e) = \langle \mathcal{L}_{\mathcal{G}\mathcal{G}}^D(B_e)(\mathbf{E}_w \cdot \mathbf{B}_e)\mathbf{E}_w + \mathcal{L}_{\mathcal{F}\mathcal{F}}^D(B_e)(\mathbf{B}_w \cdot \mathbf{B}_e)\mathbf{B}_w \rangle, \quad (29)$$

and with medium

$$\mathcal{M}^{(ph-B_e-e)}(B_e, T, \mu) = \langle \mathcal{L}_{\mathcal{G}\mathcal{G}}^{(\mu,T),D}(B_e)(\mathbf{E}_w \cdot \mathbf{B}_e)\mathbf{E}_w + \mathcal{L}_{\mathcal{F}\mathcal{F}}^{(\mu,T),D}(B_e)(\mathbf{B}_w \cdot \mathbf{B}_e)\mathbf{B}_w \rangle, \quad (30)$$

Note that $\langle \dots \rangle$ indicates the average over space-time, which applies only to the photon field since it is the only quantity dependent on space-time, as a plane wave.

The magnetization of photons exhibits the same structure in both vacuum and medium: a linear dependence on the magnetic field and a quadratic dependence on the photon fields E_w^2 and B_w^2 . The distinction between vacuum and medium arises from the expressions of the

second Lagrangian derivatives with respect to the external magnetic field. These derivatives for the vacuum correspond to finite integrals that are functions of the magnetic field: $\mathcal{L}_{\mathcal{FF}}^D$ and $\mathcal{L}_{\mathcal{GG}}^D$, while $\mathcal{L}_{\mathcal{FF}}^{(\mu,T),D}$ and $\mathcal{L}_{\mathcal{GG}}^{(\mu,T),D}$ depend on temperature, density, and magnetic field (see the appendix (A 1) and (A 2) for their expressions).

The explicit expressions are in the Appendix (A 2). For each polarization mode, $i = 2, 3$ the photon magnetization in the medium could be separated as

$$\mathcal{M}^{(2)(ph-B_e-e)} = \mathcal{L}_{\mathcal{GG}}^{(\mu),D} B_e \langle E_w^2 \rangle, \quad \mathcal{M}^{(3)(ph-B_e-e)} = \mathcal{L}_{\mathcal{FF}}^{(\mu),D} B_e \langle B_w^2 \rangle, \quad (31)$$

while for vacuum,

$$\mathcal{M}^{(2)(ph-B_e)} = \mathcal{L}_{\mathcal{GG}}^D B_e \langle E_w^2 \rangle, \quad \mathcal{M}^{(3)(ph-B_e)} = \mathcal{L}_{\mathcal{FF}}^D B_e \langle B_w^2 \rangle. \quad (32)$$

Eq. (32) reproduces the photon vacuum magnetization in the weak and strong magnetic field limits [52, 53] as follows

$$\mathcal{M}_{(ph-B_e)}^{(2),WF} = \frac{7\xi_D}{2} B_e \langle E_w^2 \rangle \hat{\mathbf{x}}_3, \quad \mathcal{M}_{(ph-B_e)}^{(3),WF} = 2\xi_D B_e \langle B_w^2 \rangle \hat{\mathbf{x}}_3, \quad (33)$$

$$\mathcal{M}_{(ph-B_e)}^{(2),SF} = \frac{\alpha_D}{3\pi} \frac{\langle E_w^2 \rangle}{B_c} \hat{\mathbf{x}}_3, \quad \mathcal{M}_{(ph-B_e)}^{(3),SF} = \frac{\alpha_D}{3\pi} \frac{\langle B_w^2 \rangle}{B_e} \hat{\mathbf{x}}_3. \quad (34)$$

Fig. (1) shows a comparison between the vacuum magnetization $\mathcal{M}^{(B_e)}$ (Eq. (28)) and the photon magnetization $\mathcal{M}^{(ph-B_e)}$ (Eq. (32)) as a function of the external magnetic field for the Dirac materials of Table I. We used $E_w/E_c = 0.01$ and $E_w = v_F B_w$ to satisfy the expansion requirement ($E_w \ll E_c$ and $B_w \ll B_c$). It is observed that the photon magnetization is always lower than the electron vacuum magnetization. While the photon magnetization varies between $10^{-6} \mu\text{T}$ and $10^{-3} \mu\text{T}$ for different materials, the contribution of electron vacuum magnetization is 3 to 6 orders of magnitude greater. In both cases, the magnetization increases with the strength of the external magnetic field and tends to remain constant when the magnetic field reaches the corresponding critical field for each material.

The contribution of the vacuum to the total magnetization is tiny at weak magnetic field scales; however, at higher magnetic field values, this contribution increases and becomes nearly constant. The photon magnetization $\mathcal{M}^{(ph-B_e)}$ of $Bi_{1-x}Sb_x$ for $B_e/B_c = 0.1$ is approximately on the order of 10^{-14} T, whereas for $Pb_{1-x}Sn_xTe$, it is on the order of 10^{-12} T for the same external magnetic field value.

Fig. (2) illustrates the behavior of electron magnetization for the Dirac materials listed in Table I. We have plotted it as a function of magnetic field and chemical potential, revealing

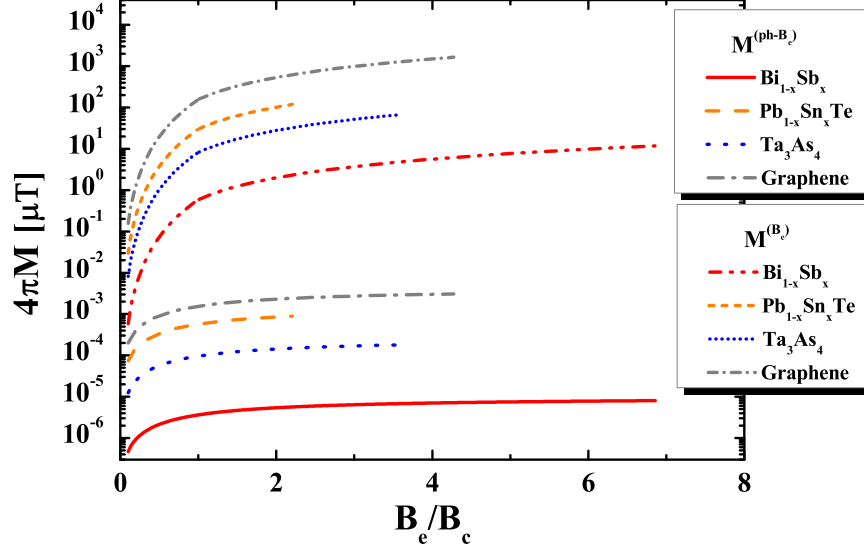


Figure 1. Vacuum magnetization $\mathcal{M}^{(B_e)}$ due to the interaction of virtual pairs with the magnetic field, (represented by the bottom four curves), and photon magnetization $\mathcal{M}^{(ph-B_e)}$ resulting from their interaction with the magnetic field through virtual pairs, (represented by the top four curves), are shown for mode $i = 2$. The magnetization is plotted as a function of the dimensionless magnetic field $b = B_e/B_c$ for each Dirac material: $Bi_{1-x}Sb_x$, $Pb_{1-x}Sn_xTe$, Ta_3As_4 , and graphene. The value of E_w is normalized using the electrical critical field, $E_w/E_c = 0.01$, and $E_w = v_F B_w$. The curves are plotted up to the maximum value of the magnetic field according to the validity in the one-loop approximation, b_{max} in Table I.

similar paramagnetic behavior across all Dirac materials. In both figures, the oscillations (a characteristic behavior of magnetized quantum gases) arise from the Hass-van Alphen effect, associated with fermion transitions between Landau levels.

The magnetization increases with the band gap and tends to stabilize when the magnetic field exceeds 4 T. Furthermore, magnetization shows a strong dependence on the increase of chemical potential across all materials. In our model, the magnetization of each material depends solely on the band gap and Fermi velocity. However, it is known that magnetization should also be influenced by the band structure (geometrical factors) and chemical composition. Then, our model tends to overestimate the magnetization, yielding large values $\mathcal{M}^{(e-B_e)} > \text{mT}$. Nevertheless, this value could be a reference for comparison with photon magnetization.

The Fig. (3) depicts the magnetization of photons interacting with the magnetic field

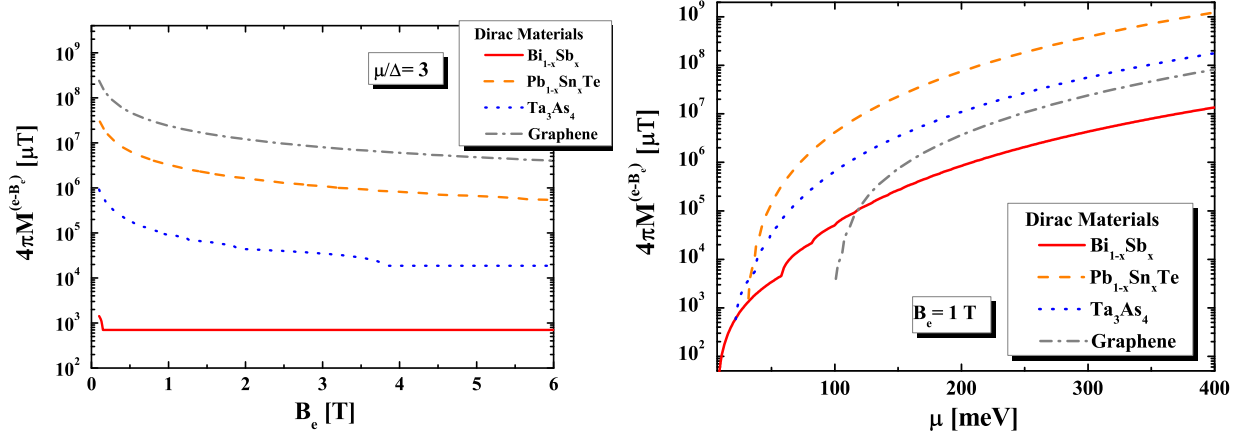


Figure 2. (Left) Magnetization of electron interacting with magnetic field $\mathcal{M}^{(e-B)}$ as a function of the magnetic field B_e in Tesla for a fixed value of $\mu/\Delta = 3$. (Right) Electron-field magnetization versus the chemical potential μ in meV for a fixed value of the external magnetic field $B_e = 1$ T. In both figures have been depicted the magnetization of studied Dirac materials: $Bi_{1-x}Sb_x$, $Pb_{1-x}Sn_xTe$, Ta_3As_4 , and graphene.

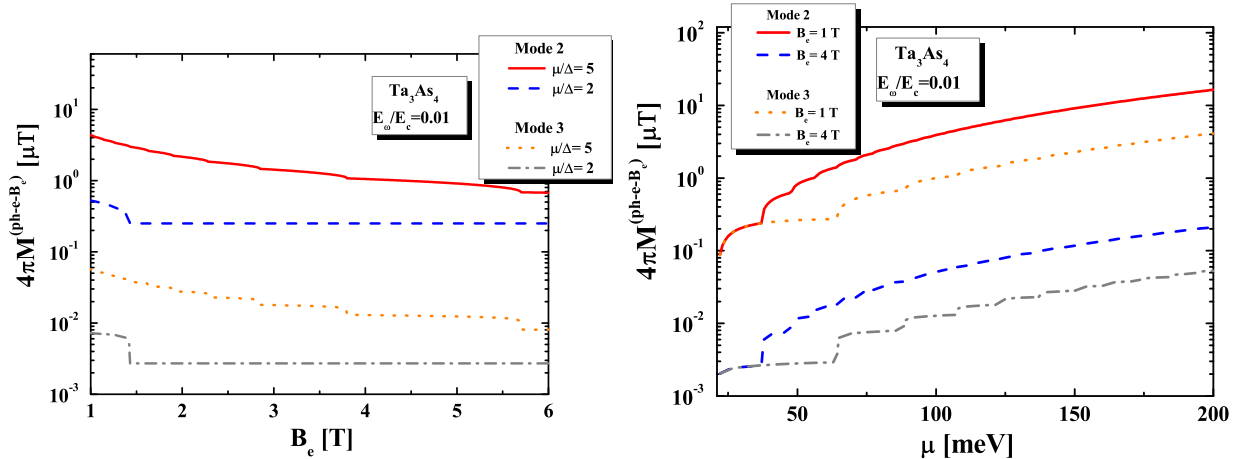


Figure 3. (Left) Magnetization of photon due to the photon interaction with magnetic field via a medium (electrons) $\mathcal{M}^{(ph-B_e-e)}$ as a function of the magnetic field B_e in tesla for a fixed value of $E_w/E_c = 0.01$ with different modes $i = 2, 3$ and chemical potentials. (Right) Magnetization of the photon interacting with the magnetic field via a medium (electrons) $\mathcal{M}^{(ph-B_e-e)}$ as a function of the chemical potential μ in meV for a fixed value of $E_w/E_c = 0.01$ with different modes $i = 2, 3$ and external magnetic fields. All figures have depicted the magnetization only for Ta_3As_4 .

through electrons $\mathcal{M}^{(ph-B_e-e)}$, using Eq. (31), as a function of the magnetic field and

chemical potential specifically for Ta_3As_4 . Both figures exhibit the Hass-van Alphen effect, resulting from the quantization of Landau levels. Similar to the $\mathcal{M}^{(e-B_e)}$, the photon magnetization also increases with the chemical potential. Nevertheless, in the figure, we can see that the photon medium magnetization $\mathcal{M}^{(ph-B_e-e)}$ match within the expected range for Dirac materials, from $0.1 \mu\text{T}$ to $10 \mu\text{T}$ [17, 28]. However, it generally varies depending on factors like the material's Fermi velocity and band gap.

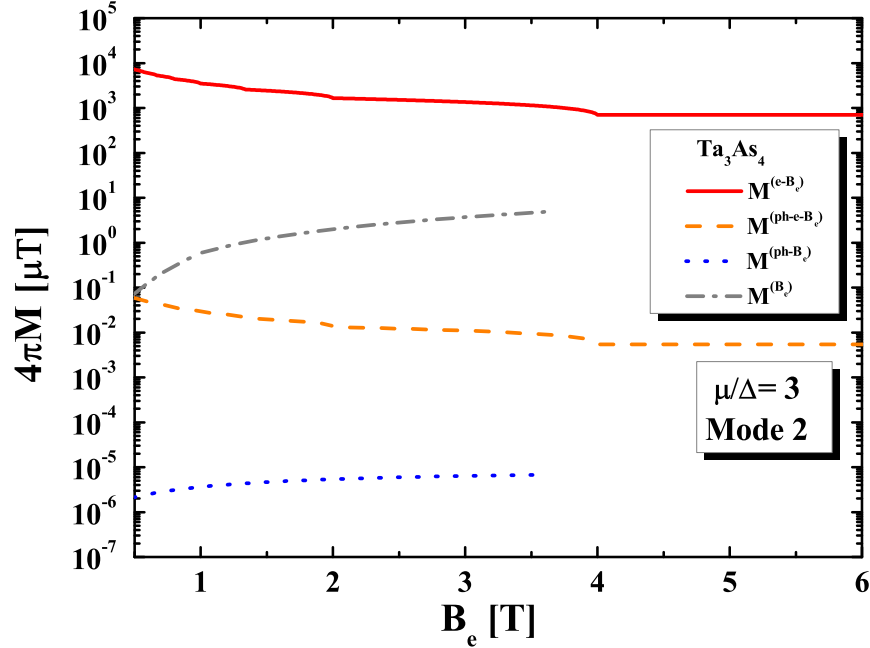


Figure 4. Comparison of the second polarization mode (2) magnetization for electron and photon considering both vacuum and medium contribution: $(\mathcal{M}^{(B_e)}, (\mathcal{M}^{(e-B_e)}, \mathcal{M}^{(ph-B_e)}, \mathcal{M}^{(ph-e-B_e)})$ as a function of the external magnetic field in Tesla for a fixed value of chemical potential $\mu/\Delta = 3$. The figures have been depicted for Ta_3As_4 . The value of E_ω is normalized using the electrical critical field, $E_\omega/E_c = 0.01$, and $E_\omega = v_F B_\omega$.

Finally, let's compare the photon and electron contributions to magnetization in Fig. (4). Here, we plot the four contributions of the total magnetization as functions of the external magnetic field for Ta_3As_4 .

We observe that the leading contribution of magnetization stems from the electron-field $\mathcal{M}^{(e-B_e)}$ being the most important in the resulting total magnetization. The relation between $\frac{\mathcal{M}^{(B_e)}}{\mathcal{M}^{(e-B_e)}} \sim 10^{-3}$ and $\frac{\mathcal{M}^{(ph-B_e)}}{\mathcal{M}^{(B_e-ph-e)}} \sim 10^{-3}$, while the magnetization due to photon propagation is just a tiny quantity in comparison with the material magnetization $\frac{\mathcal{M}^{(ph-B_e)}}{\mathcal{M}^{(e-B_e)}} \sim 10^{-9}$.

To measure this quantity, one requires greater precision and new techniques, such as those provided by superconducting quantum interference device (SQUID) magnetometry, whose sensitivity can reach up to 10^{-15} T/Hz $^{1/2}$ [17, 54]. We hope that these techniques will aid in the detection of vacuum magnetization. However, separating vacuum and medium contributions remains a challenge.

V. EFFECTIVE PHOTON MAGNETIC MOMENT

Let us study the effective magnetic moment of a photon probe propagating in a magnetized Dirac vacuum, defined from the variation of the magnetic energy $\mathcal{E} = \mathcal{M}^{(ph-B_e)} B_e = \mathcal{L}_{\mathcal{F}\mathcal{F}} \langle E_w^2 \rangle B_e^2 + \mathcal{L}_{\mathcal{G}\mathcal{G}} \langle E_w^2 \rangle B_e^2$ of the photon propagating in a Dirac vacuum with respect to the magnetic field. We translate to Dirac material language the results obtained in [27]. The explicit expression for the two modes $|\boldsymbol{\mu}_{ph}^{(2,3)}|$ reads as

$$|\boldsymbol{\mu}_{ph}^{(2)}| = \frac{\alpha_D}{16\pi} \frac{1}{b^3} \left\{ 3 - 12\zeta^{(1,1)} \left(-1, \frac{1}{2b} \right) + 3\psi \left(\frac{1}{2b} \right) \right\} + b \left[-3 + \log \Gamma \left(\frac{1}{2b} \right) \left(\frac{\pi}{b} \right)^2 + \psi^{(1)} \left(1 + \frac{1}{2b} \right) + 2b^2 \right] \frac{|\mathbf{k}_\perp|}{B_c}, \quad (35)$$

$$|\boldsymbol{\mu}_{ph}^{(3)}| = \frac{\alpha_D}{8\pi} \frac{1}{b^4} \left\{ -\psi^{(1)} \left(1 + \frac{1}{2b} \right) + b \left[4 - 4\psi \left(1 + \frac{1}{2b} \right) + 2\psi \left(\frac{1}{2b} \right) \right] + b^2 \left[4 - 2\log(2\pi) + 4\log \left(\Gamma \left(\frac{1}{2b} \right) \left(\frac{\pi}{b} \right)^{1/2} \right) \right] \right\} \frac{|\mathbf{k}_\perp|}{B_c}, \quad (36)$$

where $\psi^{(1)} = \partial_h \psi[h]$, ψ is the PolyGamma or Digamma function, (first derivative of $\ln \Gamma$). $\zeta^{(1,1)}[s, h] = \partial_h \zeta'$ with $\zeta' = \partial_s \zeta[s, h]$ and $\zeta[s, h]$ is the Hurwitz zeta function [55]. Considering the form of ψ and ζ' in weak and strong field limits (see details in [27]). For modes (2) and (3) yields $|\boldsymbol{\mu}_{ph}^{WF(2)}| = \frac{\alpha_D}{4\pi} \frac{28}{45} \frac{B_e}{B_c^2} |\mathbf{k}_\perp|$ and $|\boldsymbol{\mu}_{ph}^{WF(3)}| = \frac{4}{7} |\boldsymbol{\mu}_{ph}^{WF(2)}|$. While for strong field limit, only mode (2) contributes to the effective magnetic moment, and it goes to a constant value, $|\boldsymbol{\mu}_{ph}^{SF(2)}| = \frac{\alpha_D}{3\pi} \frac{\langle E_w^2 \rangle}{B_c}$ and $|\boldsymbol{\mu}_{ph}^{SF(3)}| = 0$. Note that the effective photon magnetic moment $|\boldsymbol{\mu}_{ph}^{SF(2)}| \sim 10^{-1} \mu_e$ is a decimal of the electron magnetic moment (μ_e), contrasting to the QED value, which is two orders lower.

In Fig. (5) left, we depict the photon's effective magnetic moment as a function of b for polarization modes (2) and (3) of Dirac materials. For comparison, we have depicted

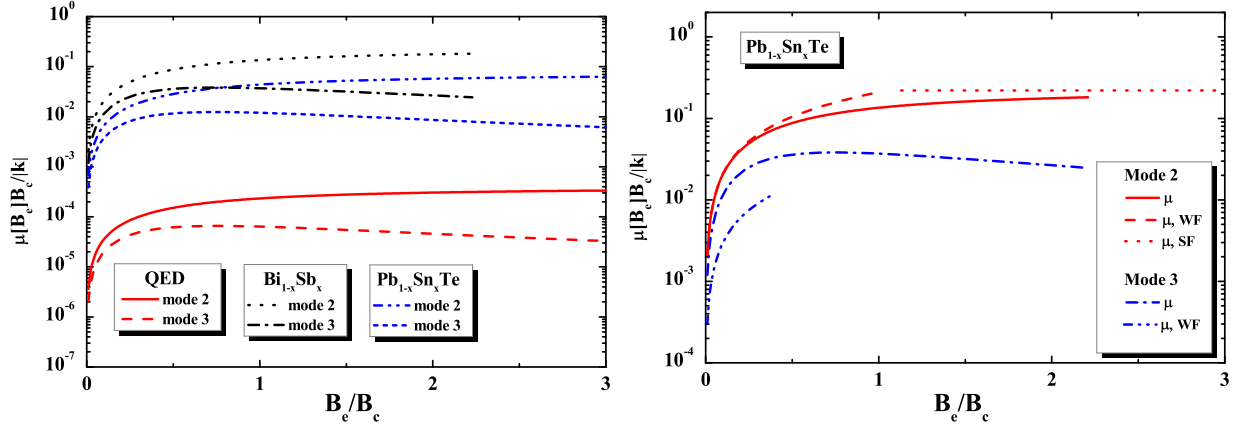


Figure 5. Photon effective magnetic moment as a function of magnetic field strength and B_e/B_c . The left figure shows the magnetic moment for two Dirac materials: $Pb_{1-x}Sn_xTe$ and $Bi_{1-x}Sb_x$. We have plotted the corresponding one for QED for both modes. For each case, the modes (2) and (3) are depicted. The right figure shows for $Pb_{1-x}Sn_xTe$ the comparison of the magnetic moment for an arbitrary value of the magnetic field with the corresponding two limits weak (dashed and dotted red line) and strong (dashed-dot-dot blue line) field limits for both modes respectively.

the magnetic moment for light propagating in a magnetized vacuum of QED. One can see that for the Dirac material, the effective magnetic moment for $Pb_{1-x}Sn_xTe$ is one order below the QED magnetic moment, while for $Bi_{1-x}Sb_x$ is three orders lower than the value of QED. On the right side of Fig. (5), we plot for $Pb_{1-x}Sn_xTe$ the effective magnetic moment, considering the results for arbitrary values of the magnetic field as well as we have plotted it for weak and strong limit for both modes. Then, for a magnetic field, $B_e \gtrsim 2B_c$ the effective magnetic moment of photons polarized on mode (2) tends asymptotically to a constant value [52, 53, 56]. Mode (3) slowly decreases with the magnetic field strength, being zero, its strong field limit value.

VI. DYNAMICS PROPERTIES OF PHOTON PROPAGATING IN A DIRAC VACUUM

We study in this section the equation of motion of the photon traveling in the Dirac vacuum $\mathcal{L}_D^{(ph-B_e)}$ using the minimum action principle, it reads as

$$\partial_\mu \left(\frac{\partial \mathcal{L}^D}{\partial f_{\mu\nu}} \right) = -\frac{1}{2}(1 - \mathcal{L}_{\mathcal{F}}^D) \partial_\mu f^{\mu\nu} + \partial_\mu \left(\frac{\mathcal{L}_{\mathcal{F}\mathcal{F}}^D}{2} (F^{\sigma\rho} f_{\sigma\rho} (F^{\mu\nu})) + \frac{\mathcal{L}_{\mathcal{G}\mathcal{G}}^D}{2} (\tilde{F}^{\sigma\rho} f_{\sigma\rho} (\tilde{F}^{\mu\nu})) \right) = 0, \quad (37)$$

where the dual tensor $\tilde{f}_{\mu\nu}$ satisfies the Bianchi equation $\partial_\mu \tilde{f}_{\mu\nu} = 0$, or second pair of Maxwell equation for \mathbf{E}_w and \mathbf{B}_w ,

$$\nabla \cdot \mathbf{B}_w = 0, \quad \frac{\partial \mathbf{B}_w}{\partial t} = -\nabla \times \mathbf{E}_w, \quad (38)$$

with $i = 1, 2, 3$. and the modified Maxwell equation in terms of constitutive vectors \mathbf{D}_w and \mathbf{H}_w are

$$\frac{\partial \mathbf{D}_w}{\partial t} = -\nabla \times \mathbf{H}_w, \quad \nabla \cdot \mathbf{D}_w = 0, \quad (39)$$

where

$$D_{w,i} = \epsilon_{ij}(B_e)E_{w,j}, \quad H_{w,i} = -(\mu^{-1})_{ij}(B_e)B_{w,j}. \quad (40)$$

In our study, we are considering an external magnetic field in $\hat{\mathbf{x}}_3$ direction $\mathbf{B}_e = B_e \hat{\mathbf{x}}_3$, and the photon propagates in $\hat{\mathbf{x}}_2$ (Fig. 6). In that case, only non-zero components of the electric permittivity and magnetic permeability tensors, are

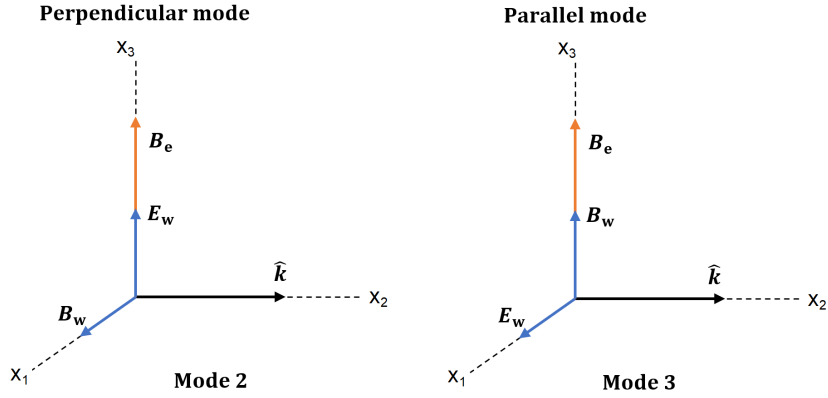


Figure 6. Two physical transverse polarization modes of the photon field, mode (2), $E_w \parallel B_e$ and mode (3), $B_w \parallel B_e$. The external magnetic field B_e in $\hat{\mathbf{x}}_3$ direction $\mathbf{B}_e = B_e \hat{\mathbf{x}}_3$, and the photon propagates in $\hat{\mathbf{x}}_2$.

$$\epsilon_{\perp} = \mu_{\perp} = 1 - \mathcal{L}_{\mathcal{F}}, \quad \epsilon_{\parallel} = (1 - \mathcal{L}_{\mathcal{F}} + 2\mathcal{F}\mathcal{L}_{\mathcal{G}\mathcal{G}}), \quad (41)$$

$$\mu_{\parallel} = (1 - \mathcal{L}_{\mathcal{F}} - 2\mathcal{F}\mathcal{L}_{\mathcal{F}\mathcal{F}}). \quad (42)$$

A. Dispersion equation of photon propagating in a Dirac vacuum

Considering the photon propagation transverse to the magnetic field (Fig. 6) of a plane wave as $\mathbf{E}_w = \mathbf{E}_0 e^{-i(\mathbf{k}_\perp \cdot \mathbf{x}_2 - \omega t)}$, from the Maxwell equations we can obtain the dispersion equation of photon as

$$(k_\perp^2 \mu_{\perp\parallel}^{-1} + \omega^2 \epsilon_{\parallel\perp}) E_w^{\parallel\perp} = 0. \quad (43)$$

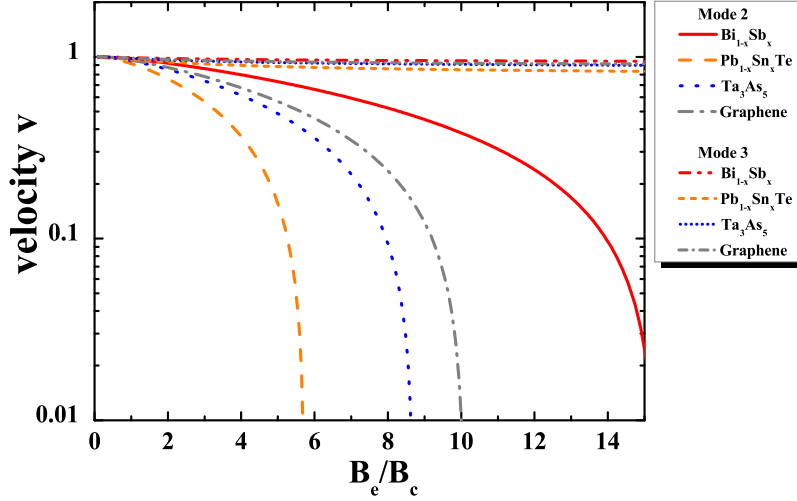


Figure 7. Phase velocity for both second and third mode of propagation of the photon as a function of the dimensionless magnetic field. The non-linear effect decreases the phase velocity with the B_e increase. We have plotted curves for four Dirac materials: $Bi_{1-x}Sb_x$, $Pb_{1-x}Sn_xTe$, Ta_3As_5 , and graphene. As we can see, the lowest velocity is obtained for $Pb_{1-x}Sn_xTe$ (dashed and short dashed orange) due to its effective fine structure constant being the highest.

The solution of Eq. (43) describes two physical transverse polarization modes of the photon field, mode (2) where the $E_w \parallel B_e$ and mode (3) $B_w \parallel B_e$.

The dispersion relation for each polarization mode has the form

$$\omega^{(2)} \simeq |\mathbf{k}_\perp| \left(1 - \frac{\mathcal{L}_{GG}^D B_e^2}{2} \right), \quad \omega^{(3)} \simeq |\mathbf{k}_\perp| \left(1 - \frac{\mathcal{L}_{FF}^D B_e^2}{2} \right), \quad (44)$$

in agreement with [52, 57, 58]. The appearance of Cotton-Mouton birefringence [1] brings the existence of two refraction indexes associated with the two different polarization modes: n_\parallel for mode (2) and n_\perp for mode (3),

$$n_{\parallel,\perp} = \frac{|\mathbf{k}_\perp|}{\omega^{(2,3)}} = \sqrt{\frac{\epsilon_{\parallel,\perp}}{\mu_{\perp,\parallel}}}. \quad (45)$$

The difference between the refraction index $\Delta n = n_{\parallel} - n_{\perp}$ takes the form

$$\Delta n = \frac{(\mathcal{L}_{GG}^D - \mathcal{L}_{FF}^D)B_e^2}{2}. \quad (46)$$

In the weak field limit, it is reduced to $\Delta n_{CM}^{WF} = 3/4\xi_D B_e^2$, instead of the strong limit $\Delta n_{CM}^{SF} = \frac{\alpha_D}{3\pi}(\frac{B_e}{B_c} - 1)$. Since the phase velocity $v_{\parallel,\perp} = 1/n_{\parallel,\perp}$, in the strong field limit the condition, $v_{\perp}^{SF} = 1 - \frac{\alpha_D}{3\pi}(\frac{B_e}{B_c}) > 0$ fixes the validity of one-loop approximation up to values of the magnetic field [40] $b \leq 3\pi/\alpha_D$.

The phase velocity as a function of the magnetic field is plotted for a second mode for four Dirac materials in Fig. (7). We have depicted curves for $Bi_{1-x}Sb_x$, graphene, Ta_3As_4 , and $Pb_{1-x}Sn_xTe$. The graphic shows that $Pb_{1-x}Sn_xTe$ has the lowest velocity with the high effective fine structure constant. The dispersion equation in weak magnetic field limit [27, 52, 59, 60] is obtained as

$$\omega^{WF,(2)} \simeq |\mathbf{k}_{\perp}| \left(1 - \frac{7}{4}\xi_D B_e^2\right), \quad \omega^{WF,(3)} \simeq |\mathbf{k}_{\perp}| (1 - \xi_D B_e^2), \quad (47)$$

while for strong magnetic field limit, the result is

$$\omega^{SF,(2)} \simeq |\mathbf{k}_{\perp}| \left(1 - \frac{\alpha_D}{3\pi} \frac{B_e}{B_c}\right), \quad \omega^{SF,(3)} \simeq |\mathbf{k}_{\perp}| \left(1 - \frac{\alpha_D}{3\pi}\right). \quad (48)$$

VII. PHOTON ENERGY-MOMENTUM TENSOR: ENERGY DENSITY, POINTING VECTOR AND RADIATION PRESSURES

The energy-momentum tensor (EMT) was calculated and widely discussed in our previous work [27] for photon propagating in a magnetic field. It was obtained from the effective Euler Heisenberg Lagrangian of QED by Hilbert method which by construction provides a symmetric EMT tensor. Besides, was proved that the EMT is gauge invariant and conserved [27]. Hilbert's method for calculating the EM tensor consists of varying the effective Lagrangian with respect to the metric tensor $g^{\mu\nu}$ and then recovering the flat space doing $g^{\mu\nu} \rightarrow \eta^{\mu\nu}$ Euclidean metric. Proceeding in a similar way that in [27] we get the EMT from the photon Lagrangian $\mathcal{L}_D^{(ph-B_e)}$. $t_H^{\gamma\rho}$ accounts for the interaction of the photon field with the background field in a Dirac vacuum, it has the form

$$t_H^{\gamma\rho} = \frac{2}{\sqrt{-g}} \frac{\delta \mathcal{L}_D^{(ph-B_e)}}{\delta g_{\gamma\rho}} \Bigg|_{g=\eta}. \quad (49)$$

Performing the derivatives and recovering the flat space, its form to Dirac material yields

$$\begin{aligned}
t^H{}^{\gamma\rho} &= (1 - \mathcal{L}_{\mathcal{F}}^D) f_{\lambda}^{\gamma} f^{\lambda\rho} + \frac{\mathcal{L}_{\mathcal{F}\mathcal{F}}^D}{2} f^{\mu\nu} F_{\mu\nu} (F^{\gamma\alpha} f_{\alpha}^{\rho} + F^{\rho\alpha} f_{\alpha}^{\gamma}) \\
&+ \frac{\mathcal{L}_{\mathcal{G}\mathcal{G}}^D}{2} f^{\mu\nu} \tilde{F}_{\mu\nu} (\tilde{F}^{\gamma\alpha} f_{\alpha}^{\rho} + \tilde{F}^{\rho\alpha} f_{\alpha}^{\gamma}) + \frac{\eta^{\gamma\rho}}{4} ((1 - \mathcal{L}_{\mathcal{F}}^D) f_{\mu\nu} f^{\mu\nu} \\
&+ \frac{\mathcal{L}_{\mathcal{F}\mathcal{F}}^D}{2} f^{\mu\nu} F_{\mu\nu} f^{\alpha\beta} F_{\alpha\beta} + \frac{\mathcal{L}_{\mathcal{G}\mathcal{G}}^D}{2} f^{\mu\nu} \tilde{F}_{\mu\nu} f^{\alpha\beta} \tilde{F}_{\alpha\beta}) \\
&+ \mathcal{L}_{\mathcal{F}}^D (F^{\gamma\alpha} f_{\alpha}^{\rho} + F^{\rho\alpha} f_{\alpha}^{\gamma}) + \frac{\eta^{\gamma\rho}}{2} \mathcal{L}_{\mathcal{F}}^D f^{\mu\nu} F_{\mu\nu}.
\end{aligned} \tag{50}$$

The external magnetic field makes EMT fully anisotropic [27]. The average of the diagonal part of the tensor corresponds to energy density and anisotropic pressures, while the non-diagonal components account for the Poynting vector.

The energy density $\langle t^{00} \rangle$ for both modes is positive [28], and the explicit expression for photon energies for both modes are,

$$\mathcal{E}_w^{\mathcal{D}(2)} \simeq (1 - \mathcal{L}_{\mathcal{F}}^D + \frac{3}{2} \mathcal{L}_{\mathcal{G}\mathcal{G}}^D B_e^2) \langle E_w^2 \rangle, \quad \mathcal{E}_w^{\mathcal{D}(3)} \simeq (1 - \mathcal{L}_{\mathcal{F}}^D - \frac{1}{2} \mathcal{L}_{\mathcal{F}\mathcal{F}}^D B_e^2) \langle E_w^2 \rangle. \tag{51}$$

However, as the Hamiltonian of the effective theory is

$$\mathcal{H}^{\mathcal{D}} = D_w E_w - \mathcal{L}_D^{\text{(ph-B}_e)} = \frac{(1 - \mathcal{L}_{\mathcal{F}}^D)}{2} (E_w^2 - B_w^2) - \frac{\mathcal{L}_{\mathcal{F}\mathcal{F}}^D}{2} (\mathbf{B} \cdot \mathbf{B}_w)^2 + \frac{\mathcal{L}_{\mathcal{G}\mathcal{G}}^D}{2} (\mathbf{B} \cdot \mathbf{E}_w)^2, \tag{52}$$

only the energy density for mode (3) becomes in the eigenvalue of the Hamiltonian [28].

The anisotropic pressures take the form

$$\begin{aligned}
p_{1,w}^{\mathcal{D}(2)} &= (1 - \frac{1}{2} \mathcal{L}_{\mathcal{G}\mathcal{G}}^D B_e^2) \langle E_w^2 \rangle, & p_{1,w}^{\mathcal{D}(3)} &= (1 - \frac{1}{2} \mathcal{L}_{\mathcal{F}\mathcal{F}}^D B_e^2) \langle E_w^2 \rangle, \\
p_{2,w}^{\mathcal{D}(2)} &= (1 - \mathcal{L}_{\mathcal{F}}^D + \frac{\mathcal{L}_{\mathcal{G}\mathcal{G}}^D B_e^2}{2}) \langle E_w^2 \rangle, & p_{2,w}^{\mathcal{D}(3)} &= (1 - \mathcal{L}_{\mathcal{F}}^D - \frac{3}{2} \mathcal{L}_{\mathcal{F}\mathcal{F}}^D B_e^2) \langle E_w^2 \rangle,
\end{aligned} \tag{53}$$

$$p_{w,\parallel}^{\mathcal{D}(2)} \simeq (1 - \frac{3}{2} \mathcal{L}_{\mathcal{G}\mathcal{G}}^D B_e^2) \langle E_w^2 \rangle, \quad p_{w,\parallel}^{\mathcal{D}(3)} \simeq (1 + \frac{1}{2} \mathcal{L}_{\mathcal{F}\mathcal{F}}^D B_e^2) \langle E_w^2 \rangle, \tag{54}$$

while the Poynting vector has the form,

$$\mathcal{P}_w^{\mathcal{D}(2)} \simeq (1 - \mathcal{L}_{\mathcal{F}}^D + \mathcal{L}_{\mathcal{G}\mathcal{G}}^D B_e^2) \langle E_w^2 \rangle, \quad \mathcal{P}_w^{\mathcal{D}(3)} \simeq (1 - \mathcal{L}_{\mathcal{F}}^D - \mathcal{L}_{\mathcal{F}\mathcal{F}}^D B_e^2) \langle E_w^2 \rangle. \tag{55}$$

We can rewrite the above quantities in terms of vacuum photon magnetization. In particular, the Poynting vector takes the form

$$\mathcal{P}_w^{\mathcal{D}(2,3)} = P_0 \pm \frac{1}{2} \mathcal{M}_D^{\text{ph-B}_e(2,3)} B_e, \tag{56}$$

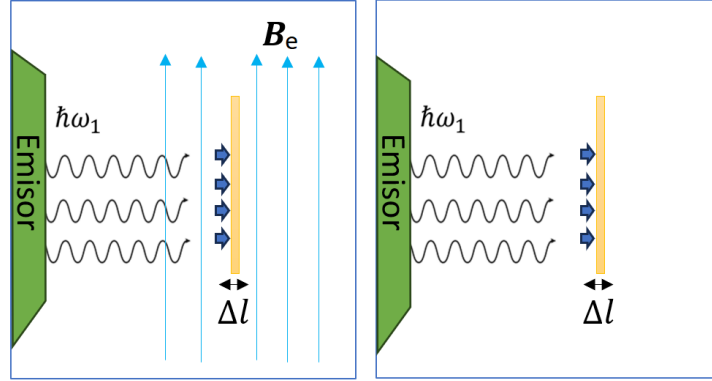


Figure 8. Proposed experiment for measuring the pressure of the radiation over the Dirac material with (left) and without (right) external magnetic field. The radiation pressures over the sheet could be measured using Eq. (56).

where P_0 contains the non-linear correction that emerges from the scalar invariant \mathcal{F} with, $P_0 = (1 - \mathcal{L}_{\mathcal{F}}^D) \langle E_w^2 \rangle$ while the second term comes from the pseudo-scalar invariant \mathcal{G} and it is proportional to the magnetization (32).

Let us highlight that Classical Electrodynamics as well as non-linear isotropic electrodynamics with Lagrangian only dependently on the scalar invariant \mathcal{F} , lead to the target pressure p_w^2 to be equal to the Poynting vector. However, the presence of the magnetic field in EH non-linear Lagrangian involves both invariant \mathcal{F} and the pseudo-scalar invariant \mathcal{G} . As we have discussed before, \mathcal{G} leads to anisotropies due to the rotation symmetry being broken. Besides, it also leads to $p_w^2 \neq \mathcal{P}_w$.

On the other hand, the radiation pressure behaves differently depending on their propagation mode. For mode (2) it is higher than the corresponding “classical pressures” while for mode (3), it becomes lower than the classical value.

Let’s imagine an experiment to detect non-linear radiation pressure. For this purpose, let’s assume a monochromatic light emitter (laser), a polarizer that allows polarization in both physical transverse modes, an external magnetic field \mathbf{B}_e in the direction \hat{x}_3 of the order of $B_e = 0.5B_c$, and a sheet of Ta_3As_4 as a 3D Dirac material of thickness Δl . The sheet is located parallel to the magnetic field in the x_1x_3 plane. The pressure of the incident beam on the sheet, would depend on $\mathcal{L}_{\mathcal{G}\mathcal{G}}^D$ or $\mathcal{L}_{\mathcal{F}\mathcal{F}}^D$ for a chosen polarization beam being greater or lower than the radiation pressure exerted by the same beam when there is no magnetic field, Fig. (8). The non-linear pressure correction will be proportional to the

magnetization. Considering the laser beam intensity, $I \sim \langle E_w^2 \rangle$ the radiation pressure will be $|\mathcal{P}_w^{D(2)}/I - 1| \approx 2.1 \times 10^{-2}$ for mode (2) and $|\mathcal{P}_w^{D(3)}/I - 1| \approx 2.2 \times 10^{-2}$ for mode (3). In the context of QED, it's notable that the correction factor is considerably smaller, roughly on the order of 10^{-5} . Specifically, in mode (2), the ratio $|\mathcal{P}_w^{QED,(2)}/I - 1| \approx 6.0 \times 10^{-5}$, while in mode (3), it's around 6.1×10^{-5} .

Of course, employing a comparable experimental setup allows for the measurement of different phases and phase velocities (birefringence) of the photon beam traversing the sheet compared to one propagating without it, both transversely propagating in the magnetic field. The birefringence is characterized by the difference between \mathcal{L}_{GG}^D and, \mathcal{L}_{FF}^D as was pointed out in Eq. (46).

VIII. CONCLUSIONS

In this paper, we extrapolate on one side and extend on the other our previous studies on photon propagation in a constant magnetic field of the QED to the context of 3D Dirac materials.

We start from the expansion up to the second order of the photon fields of the extended Euler-Heisenberg effective non-linear Lagrangian, considering low-energy photons $\omega \ll 2mc^2$ ($\omega \ll 2\Delta$) and replacing the fine-structure constant α by α_D , which depends on the Fermi velocity v_F instead of c , to describe 3D Dirac materials.

Extended effective Lagrangian to finite temperature and density is used to study the properties of a photon propagating in a magnetized medium by expanding the effective Lagrangian up to the second order in the photon fields, allowing us to study the thermodynamic properties of electrons in the presence of the magnetic field and photon propagating in 3D Dirac materials. The first term of the expansion, the zero-order term (at $E_w = B_w = 0$), is the effective Lagrangian of Euler-Heisenberg or the thermodynamic potential of electrons. So, we obtained the magnetization of the electron and the virtual pairs interacting with the magnetic field by computing the derivative of \mathcal{L}_D with respect to the magnetic field. Alternatively, the first and second-order terms of the expansion describe the properties of the photon interacting with the magnetic field via the medium and virtual pairs (vacuum).

The magnetization of a Dirac material (due to electrons) depends on α_D and the energy gap Δ . The magnetic properties have been illustrated for the Dirac materials: $Bi_{1-x}Sb_x$,

$Pb_{1-x}Sn_xTe$, Ta_3As_4 , and graphene-like, and the properties are determined by the value of the energy gap of each material.

As we expected mathematically and physically, since the medium magnetization comes from the first term of the expansion in series of effective Lagrangian, the electron magnetization is higher than the photon magnetization. In addition, the magnetization caused by the interaction of photons with the magnetic field is three or more orders of magnitude lower, depending on the material characteristics. Electron and photon magnetization preserve the paramagnetic behavior. We noted that with the increase of the magnetic field, the vacuum magnetization grows, becoming almost constant. Its contribution changes the magnetization by a quantity that could be detected at magnetic field values reachable in the laboratory. This conclusion reinforces the importance of considering the vacuum properties when studying Dirac materials.

We have obtained the dispersion law, the phase velocity, the refractive index of photons propagating in the Dirac vacuum, electric permittivity, and the magnetic susceptibility that the photon feels. The results agree with those obtained in [28]. We have discussed the energy density, pointing vector, and radiation pressures of the photon propagating transverse to the magnetic field starting from the energy-momentum tensor calculated “a la Hilbert” for effective non-linear electrodynamics for Dirac material at zero temperature and density. These quantities depend on the polarization mode. We have discussed that in our framework, the pressure target in the direction \mathbf{x}_2 does not coincide with the Poynting vector. That is a consequence of the symmetry breaking that the magnetic field produces.

Although our model for Dirac materials is simplified from the viewpoint of material science, it has all the wealth of quantum theories. It could be used to study other phenomena that appear in QED and their analogies in Dirac materials. On the other hand, the photon vacuum properties were studied for arbitrary magnetic field values, reproducing the weak and strong magnetic field limits. Besides, our study could be extended to other non-linear Lagrangians that contribute to extracting some general properties of Dirac materials.

Dirac materials present a promising avenue for probing QED properties, since non-linear corrections in magnetization, radiation pressure, and birefringence are amplified up to 10^3 times QED corrections. Dirac materials may be a medium where the vacuum properties of QED may be tested.

IX. ACKNOWLEDGMENTS

The authors thank A. to Pérez García for her contribution to our previous work. A.R.J, A.P.M, and E.R.Q. were supported by the project of No. NA211LH500-002 from AENTA-CITMA, Cuba. A.R.J. acknowledges the financial support provided by the Giersch Foundation.

-
- [1] C. Rizzo, A. Dupays, R. Battesti, M. Fouché, and G. L. J. A. Rikken. Inverse cotton-mouton effect of the vacuum and of atomic systems. *EPL (Europhysics Letters)*, 90:64003, 2010.
 - [2] A. Cadène, P. Berceau, M. Fouché, R. Battesti, and C. Rizzo. Vacuum magnetic linear birefringence using pulsed fields: status of the bmv experiment. *The European Physical Journal D*, 68, 2014.
 - [3] R. Battesti and C. Rizzo. Magnetic and electric properties of a quantum vacuum. *Reports on Progress in Physics*, 76:016401, 2012.
 - [4] H. Euler and B. Kockel. *Die Naturwissenschaften*, 23:246–247, 1935.
 - [5] W. Heisenberg and H. Euler. *Z. Phys.*, 98(11-12):714–732, 1936.
 - [6] J. Schwinger. *Phys. Rev.*, 82:664–679, 1951.
 - [7] R. Battesti and C. Rizzo. Magnetic and electric properties of a quantum vacuum. *Reports on Progress in Physics*, 76:016401, 2012.
 - [8] Yang Hailiang Cong Peitian Lai Dingguo Zhang Yuying Yang Shi, Ren Shuqing. 5 t pulsed magnetic field generator of the flash accelerator. *High Power Laser and Particle Beams*, 29(29065005):065005, 2017.
 - [9] A. Ejlli, F. D. Valle, U. Gastaldi, G. Messineo, R. Pengo, G. Ruoso, and G. Zavattini. The pvlas experiment: a 25 year effort to measure vacuum magnetic birefringence. *Physics Reports*, 871:1–74, 2020.
 - [10] S. A. Olausen and V. M. Kaspi. The mcgill magnetar catalog. *The Astrophysical Journal Supplement Series*, 212:6, 2014.
 - [11] R. Turolla, S. Zane, R. Taverna, D. Gonzalez Caniulef, R. P. Mignani, V. Testa, and K. Wu. A Comment on "A note on polarized light from Magnetars: QED effects and axion-like particles" by L.M. Capparelli, L. Maiani and A.D. Polosa. (ArXiv: 1706.02505), 2017.

- [12] A. K. Harding and D. Lai. Physics of strongly magnetized neutron stars. *Reports on Progress in Physics*, 69:2631–2708, 2006.
- [13] Yang Zhong and Chun-Bin et. al. Yang. *Advances in High Energy Physics*, 2014:1–10, 193039, 2014.
- [14] D. Tommasini, A. Ferrando, H. Michinel, and M. Seco. Precision tests of qed and non-standard models by searching photon-photon scattering in vacuum with high power lasers. *Journal of High Energy Physics*, 2009:043–043, 2009.
- [15] T. M. Jeong and J. Lee. Generation of high-intensity laser pulses and their applications. *High Energy and Short Pulse Lasers*, 2016.
- [16] M. Jirka, P. V. Sasorov, S. S. Bulanov, G. Korn, B. Rus, and S. V. Bulanov. Reaching high laser intensity by a radiating electron. *Physical Review A*, 103, 2021.
- [17] A. C. Keser, Y. Lyanda-Geller, and O. P. Sushkov. *Phys. Rev. Lett.*, 128(6):066402, 2022.
- [18] P. R. Wallace. The band theory of graphite. *Physical Review*, 71:622–634, 1947.
- [19] K. S. Novoselov et al. *Science*, 306:666–669, 2004.
- [20] A. J. Mizher, A. Raya, and C. Villavicencio. Search for fundamental physics on table top experiments with dirac–weyl materials. *Handbook of Graphene*, pages 431–466, 2019.
- [21] H. Pérez Rojas and A.E Shabad. Absorption and dispersion of electromagnetic eigenwaves of electron-positron plasma in a strong magnetic field. *Annals of Physics*, 138(1):1–35, 1982.
- [22] H. Pérez Rojas and A. E. Shabad. *Ann. Phys.*, 121:432–455, 1979.
- [23] Hugo Pérez-Rojas. *Cuba-Acad-ICT-71*, CM-P00068041, 1978.
- [24] R. G. Felipe, A. P. Martínez, and H. Perez Rojas. Relativistic quantum hall conductivity for 3d and 2d electron plasma in an external magnetic field. *Modern Physics Letters B*, 04:1103–1109, 1990.
- [25] A. P. Martínez, E. R. Querts, H. P. Rojas, R. T. Gaitán, and S. Rodríguez-Romo. 2d massless qed hall half-integer conductivity and graphene. *Journal of Physics A: Mathematical and Theoretical*, 44:445002, 2011.
- [26] L. C. Rodríguez, A. P. Martínez, H. P. Rojas, and E. R. Querts. Quantized faraday effect in (3+1)-dimensional and (2+1)-dimensional systems. *Physical Review A*, 88, 2013.
- [27] M. A. Pérez-García, A. Pérez Martínez, and E. Rodríguez Querts. Remarks on propagating waves in non-linear vacuum electrodynamics. *The European Physical Journal C*, 83(8), 2023.

- [28] M. J. Neves, P. Gaete, L. P. R. Ospedal, and J. A. Helayel-Neto. *Journal of Physics A: Mathematical and Theoretical*, 56(41):415701, 2023.
- [29] J. Cayssol. Introduction to dirac materials and topological insulators. *Comptes Rendus Physique*, 14:760–778, 2013.
- [30] S. Sahu and G. C. Rout. Band gap opening in graphene: a short theoretical study. *International Nano Letters*, 7:81–89, 2017.
- [31] S. Zhou, G. Gweon, A. V. Fedorov, P. N. First, W. A. d. Heer, D. Lee, F. Guinea, A. H. C. Neto, and A. Lanzara. Substrate-induced bandgap opening in epitaxial graphene. *Nature Materials*, 6:770–775, 2007.
- [32] M. Nevius, M. Conrad, F. Wang, A. Celis, M. N. Nair, A. Taleb-Ibrahimi, A. Tejeda, and E. H. Conrad. Semiconducting graphene from highly ordered substrate interactions. *Physical Review Letters*, 115, 2015.
- [33] G. Giovannetti, P. Khomyakov, G. Brocks, P. J. Kelly, and J. v. d. Brink. Substrate-induced band gap in graphene on hexagonal boron nitride:ab initiodensity functional calculations. *Physical Review B*, 76, 2007.
- [34] J. Jung, A. DaSilva, A. H. MacDonald, and S. Adam. Origin of band gaps in graphene on hexagonal boron nitride. *Nature Communications*, 6, 2015.
- [35] S. Villalba-Chávez, O. Mathiak, R. Egger, and C. Müller. Light-amplified landau-zener conductivity in gapped graphene monolayers: a simulacrum of photocatalyzed vacuum instability. *Physical Review D*, 108, 2023.
- [36] C. L. Kane and E. J. Mele. *Phys. Rev. Lett.*, 95:146802, Sep 2005.
- [37] Liang Fu and C. L. Kane. *Phys. Rev. B*, 74:195312, Nov 2006.
- [38] Liang Fu, C. L. Kane, and E. J. Mele. *Phys. Rev. Lett.*, 98:106803, Mar 2007.
- [39] B. Andrei Bernevig and Shou-Cheng Zhang. *Phys. Rev. Lett.*, 96:106802, Mar 2006.
- [40] W. Dittrich and H. Gies. Springer Science, Probing the Quatum Vacuum, 2000.
- [41] R. Buczko and L. Cywiński. Pbte/pbsnte heterostructures as analogs of topological insulators. *Physical Review B*, 85, 2012.
- [42] D. Hsieh, Y. Xia, D. Qian, L. A. Wray, J. H. Dil, F. Meier, J. Osterwalder, L. Patthey, J. Checkelsky, N. P. Ong, A. V. Fedorov, H. Lin, A. Bansil, D. Grauer, Y. S. Hor, R. J. Cava, and M. Z. Hasan. A tunable topological insulator in the spin helical dirac transport regime. *Nature*, 460:1101–1105, 2009.

- [43] J. C. Y. Teo, L. Fu, and C. L. Kane. *Physical Review B*, 78, 2008.
- [44] S. Xu, I. Belopolski, N. Alidoust, M. Neupane, C. Zhang, R. Sankar, S. Huang, C. Lee, G. Chang, B. Wang, G. Bian, H. Zheng, D. S. Sanchez, F. C. Chou, H. Lin, S. Jia, and M. Z. Hasan. Discovery of a weyl fermion semimetal and topological fermi arcs. *Science*, 349:613–617, 2015.
- [45] Koichi Hattori, Kazunori Itakura, and Sho Ozaki. Strong-field physics in QED and QCD: From fundamentals to applications. *Prog. Part. Nucl. Phys.*, 133:104068, 2023.
- [46] P. Elmfors, D. Persson, and B. Skagerstam. Qed effective action at finite temperature and density. *Physical Review Letters*, 71:480–483, 1993.
- [47] H. C. P. Rojas and J. L. A. Avalo. Strong magnetic fields in gauge theories. *Revista Mexicana De Física E*, 18, 2021.
- [48] R. G. Felipe, H. J. M. Cuesta, A. P. Martínez, and H. P. Rojas. Quantum instability of magnetized stellar objects. *Chinese Journal of Astronomy and Astrophysics*, 5:399–411, 2005.
- [49] F. Karbstein. Photon polarization tensor in a homogeneous magnetic or electric field. *Physical Review D*, 88, 2013.
- [50] F. Karbstein. and R. Shaisultanov. Photon propagation in slowly varying inhomogeneous electromagnetic fields. *Physical Review D*, 91, 085027, 2015.
- [51] F. Karbstein, C. Sundqvist, K. S. Schulze, I. Uschmann, H. Gies, and G. G. Paulus. Vacuum birefringence at x-ray free-electron lasers. *New Journal of Physics*, 23:095001, 2021.
- [52] H. P. Rojas and E. R. Querts. Is the photon paramagnetic? *Physical Review D*, 79, 2009.
- [53] S. Villalba-Chávez and A. E. Shabad. Qed with an external field: hamiltonian treatment of lorentz-non-invariant background as an anisotropic medium. *Physical Review D*, 86, 2012.
- [54] A. V. Gramolin, D. Aybas, D. Johnson, J. Adam, and A. O. Sushkov. Search for axion-like dark matter with ferromagnets. *Nature Physics*, 17:79–84, 2020.
- [55] V. Adamchik. *Computer Physics Communications*, 157(3):181–190, 2004.
- [56] S. R. Valluri, J. W. Mielniczuk, F. Chishtie, D. R. Lamm, and S. Auddy. *Monthly Notices of the Royal Astronomical Society*, 472:2398–2402, 2017.
- [57] A. E. Shabad and V. V. Usov. *Physical Review D*, 83, 2011.
- [58] A. W. Romero Jorge, E. Rodríguez Querts, A. Pérez Martínez, et al. *Astron. Nachr.*, 340:852–856, 2020.
- [59] H. Perez Rojas and A. E. Shabad. *Ann. phys.* 121:432–455, 1979.

- [60] A. Pérez Martínez, M. Pérez García, E. Rodríguez Querts, and A. W. Romero Jorge. In *16th Marcel Grossmann Meeting*, pages 3756–3761, 2023.
- [61] E. J. Ferrer, V. de la Incera, D. Manreza Paret, A. Pérez Martínez, and A. Sanchez. *Phys. Rev. D*, 91:085041, Apr 2015.
- [62] Ciprian Sorin Acatrinei. *Rom. J. Phys.*, 64(9-10):113, 2019.

Appendix A: Effective Lagrangian of QED at constant magnetic field from imaginary time formalism to proper time

Let us show the fundamental tricks to get the equivalent representation of $\mathcal{L}_{eff}(B_e)$ and $\mathcal{L}_{eff}(B_e, \mu, T)$ from one loop QED in presence of a magnetic field in imaginary time formalism to the Schwinger's proper method. We also show how to regularize the ultraviolet divergence of $\mathcal{L}_{eff}(B_e)$. At a constant magnetic field, the propagator of an electron in momentum space has the form

$$G_n^{-1}(\vec{p}) = \vec{p} \cdot \gamma - m, \quad (\text{A1})$$

with the notation $\vec{p} = (ip^4, 0, \sqrt{2eB_en}, p^3)$ over the Landau numbers $n = 0, 1, 2, \dots$ in Euclidean space, γ are the Gamma-matrices. In the momentum space, the effective Lagrangian has the form [47, 61]

$$\Omega(B_e, \mu, T) = -\frac{eB_e}{\beta} \left[\sum_{p_4} \int_{-\infty}^{\infty} \ln \det G_0^{-1}(\vec{p}^*) + \sum_{\sigma=\pm 1} \sum_{n=0}^{\infty} \sum_{p_4} \int_{-\infty}^{\infty} \frac{dp_3}{(2\pi)^2} \ln \det G_n^{-1}(\vec{p}^*) \right], \quad (\text{A2})$$

where $\sigma = \pm 1$ are the eigenvalues of the spin, $p_4 = i\omega_m$, ω_m is the Matsubara frequencies $\omega_m = k_B T(2m+1)\pi$ with $m = 0, 1, 2, \dots$ and, p_3 is the momentum in \hat{x}_3 -direction.

Performing the sum over Matsubara frequencies and calculating the determinants in Eq. (A2), we obtain

$$\mathcal{L}_{eff}(B_e, \mu, T) = -\frac{1}{2} \frac{eB_e}{4\pi^2} \int_{-\infty}^{\infty} dp_3 \sum_{\sigma l} |E_{\sigma n}| + \frac{eB_e}{4\pi^2} \int_{-\infty}^{\infty} dp_3 \sum_{\sigma, n} \frac{1}{\beta} \ln(1 + e^{-\beta|E_{\sigma n} - \mu|})(1 + e^{-\beta|E_{\sigma n} + \mu|}), \quad (\text{A3})$$

where $E_{\sigma n} = \sqrt{p_3^2 + m^2 + eB_e(2n+1+\sigma)}$, the first term of Eq. (A3) corresponds to the

$\mathcal{L}_{eff}(B_e)$ the second $\mathcal{L}_{eff}(B_e, \mu, T)$. Consider first $\mathcal{L}_{eff}(B_e)$

$$\mathcal{L}_{eff}(B_e) = \frac{eB_e}{4\pi^2} \int_{-\infty}^{\infty} dp_3 \sum_{\sigma, n} |E_{\sigma n}|, \quad (\text{A4})$$

using the integral representation for E

$$E = \int ds (1 - e^{-E^2 s}) s^{-3/2}. \quad (\text{A5})$$

we get

$$\mathcal{L}_{eff}(B_e) = -\frac{eB_e}{8\pi^2} \sum_{n=1}^{\infty} \sum_{\sigma=\pm 1} \int_{\epsilon}^{\infty} \frac{ds}{s^2} \left(2e^{-(m^2 + eB_e(2n + \sigma + 1))s} \right), \quad (\text{A6})$$

by performing the sum over the spin σ , we obtain the integral

$$\mathcal{L}_{eff}(B_e) = \frac{eB_e}{8\pi^2} \sum_{n=1}^{\infty} \int_{\epsilon}^{\infty} \frac{ds}{s^2} \left(2e^{-(m^2 + 2eB_e n)s} - 1 \right). \quad (\text{A7})$$

Let's now do the sum over Landau levels using

$$\sum_{n=1}^{\infty} x^n = \frac{1}{1-x}, \quad (\text{A8})$$

$\mathcal{L}_{eff}(B_e)$ yields

$$\mathcal{L}_{eff}(B_e) = \frac{eB_e}{8\pi^2} \int_{\epsilon}^{\infty} ds \frac{e^{-m^2 s}}{s^2} \left(\frac{1}{1 - e^{-2eB_e s}} - 1 \right), \quad (\text{A9})$$

in terms of hyperbolic trigonometric function, we have

$$\mathcal{L}_{eff}(B_e) = \frac{eB_e}{8\pi^2} \int_{\epsilon}^{\infty} \frac{ds}{s^2} \left(e^{-m^2 s} \coth(2eB_e s) \right), \quad (\text{A10})$$

where $\coth(2eB_e s)$ causes that the integral has an ultraviolet divergence. Expanding $\coth(2eB_e s)$ in powers of small s we obtain

$$\coth(2eB_e s) \sim \left(1 + \frac{(eB_e s)^2}{3} \right). \quad (\text{A11})$$

The prescription to regularize the integral consists of adding and subtracting divergencies terms Eq. (A11) obtaining,

$$\mathcal{L}_{eff}^R(B_e) = -\frac{1}{8\pi^2} \int_{\epsilon}^{\infty} \frac{ds}{s^3} \left(2e^{-m^2 s} \left((eB_e s) \coth(eB_e s) - 1 - \frac{(eB_e s)^2}{3} \right) \right). \quad (\text{A12})$$

To archive the effective Lagrangian for the vacuum of QED in the presence of a constant electric field is obtained from Eq. (A12) substituting $B_e = iE_e$,

$$\mathcal{L}_{eff}^R(E_e) = -\frac{i}{8\pi^2} \int_{\epsilon}^{\infty} \frac{ds}{s^3} \left(2e^{-m^2 s} \left((eE_e s) \cot(eE_e s) - 1 - \frac{(eE_e s)^2}{3} \right) \right). \quad (\text{A13})$$

The regularized effective Lagrangian Eq. (5) dependent on the electromagnetic fields can be straightforwardly obtained as \mathcal{L}_{eff}^R [62],

$$\begin{aligned} \mathcal{L}_{eff}^R(\tilde{a}, \tilde{b}) &= -\mathcal{F} - \frac{1}{8\pi^2} \int_0^{i\infty} \frac{ds}{s^3} e^{-i(m^2 - i\epsilon)s} \\ &\times \left[(es)^2 \tilde{a}\tilde{b} \coth(e\tilde{a}s) \cot(e\tilde{b}s) - \frac{(es)^2}{3} (\tilde{a}^2 - \tilde{b}^2) - 1 \right], \end{aligned} \quad (\text{A14})$$

Let us consider the second term of the effective Lagrangian Eq. (A3) dependent on temperature and density, and we check it is equivalent to Eq. (14)

$$\mathcal{L}_{eff}(B_e, \mu, T) = \frac{eB_e}{4\pi^2} \sum_{\sigma, n} \frac{a_n}{\beta} \int_{-\infty}^{\infty} dp_3 \left(\ln(1 + e^{-\beta|E_{\sigma n} - \mu|}) + \ln(1 + e^{-\beta|E_{\sigma n} + \mu|}) \right), \quad (\text{A15})$$

We first expand the logarithm in series $\ln(1+x) = \sum_{k=1}^{\infty} \frac{(-1)^{k-1}}{k} x^k$, and using the integral representation of $e^{-\beta k \sqrt{p_3^2 + m_n^2}}$

$$= -\frac{eB_e}{4\pi^2} \sum_n \frac{a_n}{\beta} \sum_{k=1}^{\infty} \frac{(-1)^k}{k} \cosh(\mu\beta k) \int_{-\infty}^{\infty} dp_3 \underbrace{e^{-\beta k \sqrt{p_3^2 + m_n^2}}}_{= \frac{\beta k}{2} \int_{-\infty}^{\infty} \frac{dt}{\sqrt{\pi} t^3} e^{-\frac{\beta k}{4t} - st}}, \quad (\text{A16})$$

$$= -\frac{eB_e}{4\pi^2} \sum_n a_n \sum_{k=1}^{\infty} (-1)^k \cosh(\mu\beta k) \int_{-\infty}^{\infty} dp_3 \int_0^{\infty} \frac{dt}{\sqrt{\pi} t^{3/2}} e^{-\frac{\beta}{4t} - (p_3^2 + m_n^2)t}, \quad (\text{A17})$$

$$= -\frac{eB_e}{4\pi^2} \sum_n a_n \sum_{k=1}^{\infty} (-1)^k \cosh(\mu\beta k) \int_{-\infty}^{\infty} \frac{dt}{\sqrt{\pi} t^{3/2}} e^{-\frac{\beta^2 k^2}{4t} - m_n^2 t} \left(\frac{-\beta k}{2} \right) \underbrace{\int_0^{\infty} dp_3 e^{-tp_3^2}}_{\sqrt{\pi/t}}, \quad (\text{A18})$$

$$= \frac{eB_e}{8\pi^2} \sum_{k=1}^{\infty} (-1)^k \cosh(\mu\beta k) \int_0^{\infty} \frac{dt}{t^2} e^{-\frac{\beta^2 k^2}{4t} - m_n^2 t} \underbrace{\sum_{n=0}^{\infty} a_n e^{-2eB_e n t}}_{\coth(eB_e t)}, \quad (\text{A19})$$

$$= \frac{eB_e}{8\pi^2} \sum_{k=1}^{\infty} (-1)^k \cosh(\mu\beta k) \int_0^{\infty} \frac{dt}{t^2} e^{-\frac{\beta^2 k^2}{4t} - m_n^2 t} \coth(eB_e t) \quad (\text{A20})$$

1. Lagrangian derivatives at $T = \mu = 0$

At $T = \mu = 0$ the integrals of Lagrangian derivatives $\mathcal{L}_{\mathcal{F}, \mathcal{FF}, \mathcal{GG}}^f$ are reduced to the previously calculated in [27, 40], after perform the integration their explicit form remain

$$\begin{aligned}
\mathcal{L}_{\mathcal{F}}^D &= \left. \frac{\partial \mathcal{L}}{\partial \mathcal{F}} \right|_{f=0} = \frac{\alpha_D}{2\pi\mu_0} \left(-\frac{1}{3} + 2h_D^2 + 8\zeta'(-1, h_D) - 4h_D \ln \Gamma(h_D) + 2h_D \ln h_D - \frac{2}{3} \ln h_D + 2h_D \ln 2\pi \right), \\
\mathcal{L}_{\mathcal{F}\mathcal{F}}^D &= \left. \frac{\partial^2 \mathcal{L}}{\partial^2 \mathcal{F}} \right|_{f=0} = \frac{\alpha_D}{2\pi\mu_0 B^2} \left(\frac{2}{3} + 4h_D^2 \psi(1 + h_D) - 2h_D - 4h_D^2 - 4h_D \ln \Gamma(h_D) + 2h_D \ln 2\pi - 2h_D \ln h_D \right), \\
\mathcal{L}_{\mathcal{G}\mathcal{G}}^D &= \left. \frac{\partial^2 \mathcal{L}}{\partial^2 \mathcal{G}} \right|_{f=0} = \frac{\alpha_D}{2\pi\mu_0 B^2} \left(-\frac{1}{3} - \frac{2}{3} (\psi(1 + h_D) - 2h_D^2 + (3h_D)^{-1}) + 8\zeta' \right). \tag{A21}
\end{aligned}$$

where $h_D = \frac{\Delta^2}{eB_e}$. Similar results of the integrals Eq.(A21) are obtained for a pure background electric field and for the background of an orthogonal electric and magnetic field, doing $h_D \rightarrow \frac{\Delta^2}{2e\sqrt{\mathcal{F}}}$.

2. Derivatives Lagrangian $T = 0, \mu \neq 0$

Let's compute the integrals for $\mathcal{L}_{\mathcal{F}, \mathcal{F}\mathcal{F}, \mathcal{G}\mathcal{G}}^{(\mu, T), D}$. To achieve this, we take advantage of the equivalence in one-loop approximation between the effective Euler-Heisenberg (EH) Lagrangian in the infrared regime (as presented in this paper) and the off-shell photon's polarization operator [57].

The equivalence between both procedures is given by relations between the coefficients of the quadratic effective EH Lagrangian ($\mathcal{L}_{\mathcal{F}, \mathcal{F}\mathcal{F}, \mathcal{G}\mathcal{G}}^{(\mu, T), D}$) and the eigenvalues of the polarization operator (see details in [57] Eq. 21). This equivalence may be extended to the temperature and density correction term of the EH-effective Lagrangian. The relationship between the eigenvalues of the polarization operator $\Pi_{\mu\nu}$ and the Lagrangian derivatives is the following

$$2\mathcal{F}\mathcal{L}_{\mathcal{F}}^{(\mu, T), D} = \kappa_1|_{k \rightarrow 0}, \tag{A22}$$

$$2\mathcal{F}\mathcal{L}_{\mathcal{F}\mathcal{F}}^{(\mu, T), D} = (\kappa_1 - \kappa_3)|_{k \rightarrow 0}, \tag{A23}$$

$$2\mathcal{F}\mathcal{L}_{\mathcal{G}\mathcal{G}}^{(\mu, T), D} = (\kappa_1 - \kappa_2)|_{k \rightarrow 0}. \tag{A24}$$

Then, we start from the eigenvalues of the polarization operator at finite temperature and density $\kappa_1, \kappa_2, \kappa_3$ obtained in [59], in the degenerate limit (zero temperature and finite den-

sity), obtaining

$$\begin{aligned}\mathcal{L}_{\mathcal{F}}^{(\mu),D}(\mu, B_e) &= -\frac{\alpha_D}{2\pi B_e B_c} \sum_{n=0}^{n_\mu} a_n \int \frac{dp_3 \theta(\mu - E_{\sigma n})}{\sqrt{p_3^2 v_F^2 + \Delta_n^2}} \\ &= -\frac{\alpha_D}{2\pi B_e B_c v_F} \sum_{n=0}^{n_\mu} a_n \ln \left(1 + \frac{2p_F v_F (\mu + p_F v_F)}{\Delta_n} \right),\end{aligned}\tag{A25}$$

$$\mathcal{L}_{\mathcal{F}\mathcal{F}}^{(\mu),D}(\mu, B_e) = \frac{\mathcal{L}_{\mathcal{F}}^\mu}{2},\tag{A26}$$

$$\begin{aligned}\mathcal{L}_{\mathcal{G}\mathcal{G}}^{(\mu),D}(\mu, B_e) &= -\frac{\alpha_D}{4\pi B_e B_c} \sum_{n=0}^{n_\mu} a_n \left(\int \frac{dp_3 \theta(\mu - E_{\sigma n})}{\sqrt{p_3^2 v_F^2 + \Delta_n^2}} - 4 \int \frac{dp_3 \theta(\mu - E_{\sigma n})}{E_{\sigma n}^3} \right), \\ &= -\frac{\alpha_D}{4\pi B_e B_c v_F} \sum_{n=0}^{n_\mu} a_n \left(\ln \left(1 + \frac{2p_F v_F (\mu + p_F v_F)}{\Delta_n} \right) - 4 \frac{p_F}{\mu} \right).\end{aligned}\tag{A27}$$